Department of Bioproducts and Biosystems

Lignocellulosic building blocks for aerogel and nanocomposite applications

Muhammad Farooq

Aalto University

DOCTORAL DISSERTATIONS

Aalto University publication series
DOCTORAL DISSERTATIONS 69/2021

Lignocellulosic building blocks for aerogel and nanocomposite applications

Muhammad Farooq

A doctoral dissertation completed for the degree of Doctor of Science (Technology) to be defended, with the permission of the Aalto University School of Chemical Engineering, at a public examination held at the lecture hall Ke1 of the school on 2nd June 2021 at 12 noon.

Aalto University
School of Chemical Engineering
Department of Bioproducts and Biosystems
Bioproduct Chemistry

Supervising professor
Professor Monika Österberg, Aalto University, Finland

Thesis advisors
Assistant Professor Mika Sipponen, Stockholm University, Sweden
Doctor Juan José Valle Delgado, Aalto University, Finland

Preliminary examiners
Docent Olena Sevastyanova, KTH Royal Institute of Technology, Sweden
Associate Professor Tiina Nypelö, Chalmers University of Technology, Sweden

Opponents
Professor Lennart Bergström, Stockholm University, Sweden

Aalto University publication series
DOCTORAL DISSERTATIONS 69/2021

ISBN 978-952-64-0382-3 (printed)
ISBN 978-952-64-0383-0 (pdf)
ISSN 1799-4934 (printed)
ISSN 1799-4942 (pdf)
http://urn.fi/URN:ISBN:978-952-64-0383-0

Unigrafia Oy
Helsinki 2021

Finland

Printed matter
4041-0619

Aalto University

Abstract

Aalto University, P.O. Box 11000, FI-00076 Aalto www.aalto.fi

Author
Muhammad Farooq

Name of the doctoral dissertation
Lignocellulosic building blocks for aerogel and nanocomposite applications

Publisher School of Chemical Engineering

Unit Department of Bioproducts and Biosystems

Series Aalto University publication series DOCTORAL DISSERTATIONS 69/2021

Field of research Bioproduct Technology

Manuscript submitted 3 April 2021 **Date of the defence** 2 June 2021

Permission for public defence granted (date) 30 April 2021 **Language** English

☐ **Monograph** ☒ **Article dissertation** ☐ **Essay dissertation**

Abstract

Each new dawn is marking our success in the field of science and technology, fortifying our knowledge, but at the same time risks associated with the plethora of environmental challenges in the form of climate change, air and ocean pollution and use of fossil fuels are rapidly growing as well. In these circumstances, a paradigm shift from a fossil-based society to a greener, bio-based one is highly encouraging. The growing concerns associated with the end of life of plastics and new legislation from governments have generated a demand for lignocellulosic materials. Lignocellulosic biomass, consisting of the natural polymers, cellulose and lignin, have been recognized as possible raw material for innovative bio-based products with added value.

In this work, two major components of lignocellulosic biomass, cellulose at its nanoscale morphology, termed as "cellulose nanofibrils" (CNF), obtained via fibrillation and "colloidal lignin nanoparticles" (CLPs), transformed through the self-assembly process of crude lignin, have been utilized as building block materials for diverse practical applications. Among different enticing features of CNF, its low thermal conductivity was emphasized by preparing flame-retardant CNF aerogels. The readily available sodium bicarbonate proved itself as an effective eco-friendly flame-retardant. Mixing CNF with sodium bicarbonate enabled the production of low-density aerogels with self-extinguishing behavior upon the removal of the flame source and decreased combustion velocity while retaining the good insulating properties of the aerogels. Due to the challenges posed by the hydrophilic nature of CNF, the second nano component of lignocellulosic biomass, "CLPs" were examined for their interfacial properties using surface-sensitive methods. The gained fundamental understanding was put forth to develop strong nanocomposites from CNF and CLPs. Both CLPs and CNF demonstrated excellent suitability for water-based systems and the prepared nanocomposite films showed a significant increase in toughness at an optimum ratio between CLPs and CNF. In response to the hydrophilic surface character of CNF and CLPs, the following work utilized a water-based PU system in combination with CNF to selectively hydrophobized one side of the nanocomposite film, retaining the hydrophilicity of the other side. The further exploration of CLPs as low-cost enzyme carriers for aqueous ester synthesis exhibited 95% of the synthetic activity under a high aqueous reaction medium. Enzyme immobilized c-CLPs demonstrated excellent stability under esterification conditions, reusability, and high molar yield of esterification reaction yield.

In conclusion, we demonstrated that nano-morphologies of CNF and CLPs provide a new toolbox for designing products of biological-origin with the possibility to functionalize and modify the interface between different building components.

Keywords Lignocellulose, Colloidal lignin particles, Aerogels, Insulation, Nanocomposites

ISBN (printed) 978-952-64-0382-3 **ISBN (pdf)** 978-952-64-0383-0

ISSN (printed) 1799-4934 **ISSN (pdf)** 1799-4942

Location of publisher Helsinki **Location of printing** Helsinki **Year** 2021

Pages 171 **urn** http://urn.fi/URN:ISBN:978-952-64-0383-0

Acknowledgments

This research work was carried out at the Bioproduct Chemistry group, led by Prof. Monika Österberg, Department of Bioproducts and Biosystems at Aalto University. The research was funded by Aalto University, Novo Nordisk (SUS-CELL), and by European Union and Bio-Based Industries consortium (EU-BBI) (Zelcor). I am grateful for their financial support in making this research possible.

Here comes that moment to thank everyone that contributed to this incredible Ph.D. adventure, in which I encountered plenty of failures and few instances of success. Firstly, I would like to express my sincere gratitude to my supervisor Professor Monika Österberg for the continuous support throughout the doctoral studies and research, for her patience, motivation, and extensive knowledge. I would like to mention her patience again. Her guidance, positive encouragement, and warm spirit helped me in all the time of research and writing of this thesis. I could not have imagined having a better advisor and mentor for my Ph.D. study. Besides my supervisor, I would like to thank my thesis advisors: Assistant Professor Mika H. Sipponen and Dr. Juan José Valle Delgado for their insightful comments and encouragement, but also for the hard question which incented me to widen my research from various perspectives. I was fortunate to learn from Mika H. Sipponen to design and conduct my research appropriately to answer the research questions.

I thank my fellow research group members for the stimulating discussions, for the long evenings we were working together before deadlines, and for all the fun we have had in the last four years. I admire the research atmosphere, Professor Monika Österberg has provided within our research group which allows us to question, collaborate and learn regularly.

Last but not the least, I would like to thank my family: my parents, my wife, my son, and my brothers and sister for supporting me spiritually throughout writing this thesis and my life in general.

Helsinki, 8 March 2021
Muhammad Farooq

Contents

List of Abbreviations and Symbols

AFM	atomic force microscope
AL	alkali lignin
BA	boric acid
BTCA	1,2,3,4-butane tetracarboxylic acid
c-CLPs	cationic colloidal lignin particles
CLPs	colloidal lignin nanoparticles
CLSM	confocal laser scanning microscopy
CNC	cellulose nanocrystals
CNF	cellulose nanofibrils
C-NMR	carbon-13 nuclear magnetic resonance
DDMA	di-dodecyl dimethylammonium bromide
DMF	N, N-dimethylformamide
DSC	differential scanning calorimetry
DVS	dynamic vapor sorption
EG	ethylene glycol
EMC	equilibrium moisture content
FESEM	field emission scanning electron microscopy
FTIR	fourier-transform infrared spectroscopy
GO	graphene oxide
GTMAC	glycidyl tetramethyl ammonium chloride
HAP	hydroxyapatite
HiC	humicola insolens cutinase
LNPs	lignin nanoparticles
MA	melamine-formaldehyde

MDPA	N-methylol dimethylphosphonopropionamide
MFC	microfibrillated cellulose
MMT	sodium montmorillonite
MoS_2	molybdenum disulfide
NFC	nanofibrillated cellulose
NMR	nuclear magnetic resonance
OS	organosolv
PGN	phosphorus-hybridized graphene nanosheets
PLA	polylactic acid
PLL	poly-L-lysine
PS	polystyrene
PU	polyurethane
PVA	polyvinyl alcohol
QCM-D	quartz crystal microbalance with dissipation monitoring
RH	relative humidity
RMS	root mean squared
SBC	sodium bicarbonate
SDS	sodium dodecyl sulfate
SFMs	scanning force microscope
SL	soda lignin
SPMs	scanning probe microscopes
TGA	thermogravimetric analyzer
THF	tetrahydrofuran
TP	thermoporometry
UV	ultraviolet
XRD	x-ray diffraction
λ	thermal conductivity

List of Publications

This doctoral dissertation consists of a summary of the following publications which are referred to in the text by their numerals

1. Farooq, M., Sipponen, M. H., Seppälä, A., & Österberg, M. (2018). Eco-friendly Flame-Retardant Cellulose Nanofibril Aerogels by Incorporating Sodium Bicarbonate. *ACS Applied Materials & Interfaces*, *10*(32), 27407–27415. DOI:10.1021/acsami.8b04376

2. Farooq, M., Tao, Z., Valle-Delgado, J. J., Sipponen, M. H., Morits, M., & Österberg, M. (2020). Well-Defined Lignin Model Films from Colloidal Lignin Particles. *Langmuir*, *36*(51), 15592–15602. DOI: 10.1021/acs.langmuir.0c02970

3. Farooq, M., Zou, T., Riviere, G., Sipponen, M. H., & Österberg, M. (2018). Strong, Ductile, and Waterproof Cellulose Nanofibril Composite Films with Colloidal Lignin Particles. *Biomacromolecules*, *20*(2), 693–704. DOI: 10.1021/acs.biomac.8b01364

4. Sethi, J., Farooq, M., Österberg, M., Illikainen, M., & Sirviö, J. A. (2018). Stereoselectively Water Resistant Hybrid Nanopapers Prepared By Cellulose Nanofibers And Water-Based Polyurethane. *Carbohydrate Polymers*, *199*, 286–293. DOI: 10.1016/j.carbpol.2018.07.028

5. Sipponen, M. H., Farooq, M., Koivisto, J., Pellis, A., Seitsonen, J., & Österberg, M. (2018). Spatially Confined Lignin Nanospheres For Biocatalytic Ester Synthesis In Aqueous Media. *Nature Communications*, *9,2300*. DOI: 10.1038/s41467-018-04715-6

Author's Contribution

Publication I: "Eco-friendly Flame-Retardant Cellulose Nanofibril Aerogels by Incorporating Sodium Bicarbonate"

M.F. conducted the experiments and analyzed the data in collaboration with M.H.S. and M.Ö. A.S. helped with performing thermal conductivity measurements. M.F. wrote the manuscript with inputs from all of the authors. All of the authors discussed the results and read and approved the manuscript.

Publication II: "Well-Defined Lignin Model Films from Colloidal Lignin Particles"

M.F. and Z.T. designed the experiments with M.H.S., J.J.V.-D., M.M., and M.Ö. Experiments and data analysis were performed by M.F. and Z.T. in collaboration with J.J.V.-D. and M.Ö. M.F. drafted the manuscript with support from all authors. All authors discussed the results, commented, and approved the manuscript.

Publication III: "Strong, Ductile, and Waterproof Cellulose Nanofibril Composite Films with Colloidal Lignin Particles"

M.F. designed the experiments with T.Z., M.H.S., and M.Ö. Experiments and data analysis was performed by M.F. in collaboration with M.H.S and M.Ö. T.Z. contributed to the sample preparation and optimization. G.R conducted the spectrophotometric transmittance measurements and antioxidant characterization. M.F wrote the manuscript with input from all authors. All authors discussed the results, read, and approved the manuscript.

Publication IV: "Stereoselectively Water-Resistant Hybrid Nanopapers Prepared By Cellulose Nanofibers And Water-Based Polyurethane"

J.S designed the experiments with M.F. Experiments and data analysis was performed by J.S in collaboration with M.F. All authors discussed the results, read, and approved the manuscript.

Publication V: "Spatially Confined Lignin Nanospheres For Biocatalytic Ester Synthesis In Aqueous Media"

M.H.S. designed, performed, and analyzed the experiments. M.F. prepared samples for FESEM, performed FE-SEM imaging, and assisted with CLSM imaging. J.K. was responsible for NMR analysis of lignin and A.P. purified and

characterized HiC. J.S. carried out cryo-sectioning and TEM imaging of the alginate beads. M.H.S and M.Ö. co-wrote the manuscript. All authors discussed the results and commented on the manuscript of the article

1. Introduction

The plethora of ecological insecurities faced today is significantly higher than ever before, affecting biosphere integrity and threatening our very own existence. Considering this scenario, the implementation of sustainability-oriented strategies such as circular economy, green economy, and bioeconomy, intended to transform the current fossil-based, linear economy into an efficient, circular one, has been well received by the scientific community and as well as from industry.[1,2] This transition towards circular bioeconomy is anticipated to provide a window of opportunity to address interlinked challenges like fossil resource dependence, natural resource scarcity, climate change, and food security by employing greener manufacturing methodologies and use of renewable bio-resources. [3,4]

Material development has played a fundamental role in the advancement of our society. In today's world, new advancements in material development are emerging frequently. The discovery of oil played a pivotal role in the industrial revolution and at the same time, the availability of the plentiful carbon atoms extracted from oil intensified the production of synthetic polymers and plastics. When we learned how to synthesize and manipulate the properties of plastics, it became a significant part of our lives. Plastics offer vindicating benefits over glass, metal, and wood such as moldability, durability, versatility, and reusability.

The growing concerns associated with the end of life of plastics,[5] their use in short-lived applications with a poor design for re-use the hidden crisis of micro plastics[5], have collectively prompted the pursuit of sustainable alternatives. Bio-based materials either obtained from plant biomass or marine resources instead of from fossil fuel have gained considerable attention.[6,7] Bio-based materials are replacing conventional plastics in several applications such as packaging, catering products, consumer electronics, and automotive.[8]

The necessity of sustainable development and emerging trends have put the forest sector center stage. A multitude of product opportunities can be offered from lignocellulosic feedstock and its side streams.[9] Lignocellulosic biomass, consisting of the most abundant natural polymers such as cellulose, hemicellulose, and lignin has been recognized for the development of innovative bio-based products with higher added value.[10–12] Lignocellulose at its nanoscale

morphology, termed as “Cellulose nanofibrils” (CNF) and “Colloidal lignin nanoparticles” (CLPs) which are obtained from crude lignin via dissolution and self-assembly, has enticing features that can be utilized in various applications. CNF possesses a high aspect ratio along with remarkable tensile properties, low thermal conductivity, non-toxicity, and tunability.[12–15] These multifunctional attributes have earned their place in nanocomposites, aerogels, drug delivery, biosensing, and enzyme immobilization. The use of CNF in water-based systems is fairly convenient due to its surface properties. However, the presence of hydroxyl groups on the surface of CNF causes hindrance to its dispersion in hydrophobic mediums and results in poor matrix/fiber interface, which limits its application in combination with biobased hydrophobic polymers. [16] To overcome this challenge surface modification strategies[17–21] are often employed. However, these extensive chemical modifications are not always environmentally friendly and may hamper biodegradability.[22] A more natural and sustainable solution comes from lignin, the second largest constituent of the lignocellulosic biomass. The conversion of crude lignin into colloidal lignin particles overcomes the hurdles posed by its complex structural heterogeneity. The resulting nanoparticles are potentially lucrative due to their nano-scale morphology and surface characteristics.[23–25]

The potential contribution of lignocellulosic biomass to the bioeconomy is expected to revolutionize the forest industry. Forests are Finland’s most valuable natural resource and their efficient utilization will not only propel the business growth through encouraging innovations and investment opportunities but will also help to attain Finland’s 2035 carbon neutrality goal.

2. Scope of thesis

This thesis is comprised of the results obtained in 5 articles. The prime objective was to harness the collective properties of CNF and CLPs as building blocks materials for diverse practical applications. To pursue these goals, Publication I explores the application prospect of porous CNF networks in the form of aerogels as thermal insulation material, owing to the low thermal conductivity of CNF. To enhance their flame-retardancy, sodium bicarbonate (SBC) was embedded in the CNF aerogels. Thermal and flammability properties were evaluated to confirm their suitability as insulation materials.

In Publication II, to efficiently harness the potential of CLPs for nanocomposite application, their interfacial and surface properties were examined. Model surfaces, in combination with surface-sensitive tools, were employed to probe the stability of CLPs at various pHs and the interactions between the CLPs and cationic polymers. The fundamental understanding obtained was employed to enhance the properties of cellulosic nanocomposites prepared by utilizing spherical lignin particles in Publication III. The results acquired indicated that the well-defined surface chemistry and morphology of CLPs allow them to readily disperse in CNF suspensions forming nanocomposite films with nearly double the toughness compared to a CNF film without lignin. In Publication IV, another nanocomposite system based on polyurethane (PU) and CNF was prepared using a water-based method. The foremost objective of this study was to improve the wet mechanical properties of the CNF network. The prepared nanocomposites demonstrated hydrophobic character on the PU-rich surface and hydrophilic features on the CNF-rich surface.

In the last work (Publication V), the large specific surface area of CLPs, because of their spherical morphology and their nano-dimensions, was exploited by using CLPs as low-cost enzyme carriers for aqueous ester synthesis. Lipase M enzyme was adsorbed onto CLP surfaces coated with cationic lignin. The enzyme immobilization was accomplished by entrapping the enzyme-c-CLP complexes in calcium alginate. Overall, the presented work demonstrates the potential of CLPs and CNF for value-added applications as a replacement for synthetic polymers.

3. Fundamentals

3.1 Lignocellulosic biomass

Plants represent 80% (≈450 Gt) of the total biomass (550 Gt) present on earth, consisting of woody, nonwoody, and grass biomass.[26] Wood in its essence is nature's composite, providing plants their structural rigidity.[27] Wood mainly consists of three types of carbon-based polymers, the polysaccharides cellulose, hemicellulose, along with aromatic lignin, collectively termed lignocellulosic biomass.[28] Cellulose, a linear polymer of D-glucopyranose monomeric units exists in the form of crystalline microfibrils.[29–31] The hemicellulose, consisting of different sugars, such as hexoses and pentoses, is attached to cellulose in close proximity.[28,29] Lignin being the third major component of lignocellulosic biomass, is naturally a linear oligomer, which surrounds the cellulose and hemicellulose as a protective constituent.[32–34] Cellulose and hemicellulose make up to approximately 70% and lignin roughly 25% of the dry weight of lignocellulose biomass.[35] Few examples of lignocellulosic biomass and their cell wall compositions are depicted in Figure 1.

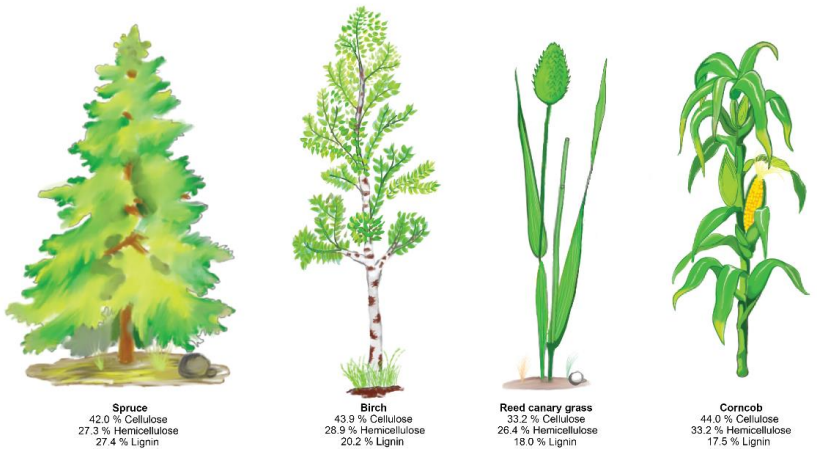

Figure 1. Examples of lignocellulosic biomass and their respective cell wall compositions. (Data is based on the ref. [36–39])

3.2 Cellulose: From macroscopic fibers to nanocellulose

At the molecular level, cellulose is an unbranched homopolysaccharide composed of β-D-glucopyranose units connected through (1→4) glycosidic bonds.[31,40] Glucopyranose rings adopt a chair conformation designated $^4C_1$ and are rotated with respect to each other, while all the hydroxyl groups are in equatorial positions with respect to the pyranose ring plane.[40,41] Cellulose chains take the form of sheets and run parallel in cellulose I crystal, stacked on top of each other forming a three-dimensional crystal structure.[41,42]

The readily available hydroxyl groups in the cellulose chain participate in strong inter and intramolecular hydrogen bonds (Figure 2c). [40,43] The intermolecular hydrogen bonds keep the sheets together, whereas intramolecular hydrogen bonds give rigidity to the cellulose chain.[44] Several parallel cellulose chains form the rudimentary supramolecular unit of cellulose known as the microfibril.[45] The degree of polymerization of cellulosic chains for wood-derived cellulose is ~10 000 AGUs (anhydroglucose units) and 15 000 units, for cotton-derived cellulose.[40] The diameter of a microfibril revealed by X-ray diffraction and Carbon-13 nuclear magnetic resonance (C-NMR) spectroscopy is approximately 2.4 to 3.6 nm,[46] whereas the length of the microfibril is roughly tens of micrometers,[47] largely depending on the cellulose source. According to the crystallographic information, the cellulose present within the microfibrils is not entirely crystalline; rather it consists of crystalline regions and disordered regions, indicated in Figure 2b. Crystalline regions are predominant, but the order is frequently disrupted by disordered regions, periodically distributed across the microfibrils.[48]

In context of the arrangement of cellulose chains and their numbers in a cellulose microfibril, several cross-sectional structure models have been proposed. Based on the organization of the rosette in biosynthesis and the evidence collected from XRD and microscopic data, it was long thought that microfibrils consist of (6 × 6) cellulose chains arranged in an irregular rectangle.[49] Later, an alternative 6 × 6 (hexagonal) model[50] based on atomic force microscopy (AFM) data. A 24 chain model[51] based on diffraction, NMR, and Fourier-transform infrared spectroscopy (FTIR) data has also been proposed. Both of the 6x6, the rectangular[49] and hexagonal,[50] models are frequently employed for molecular modeling. However, recent molecular simulations have further convinced the researchers to reduce the number of chains to 18, as depicted in Figure 2d.[52]

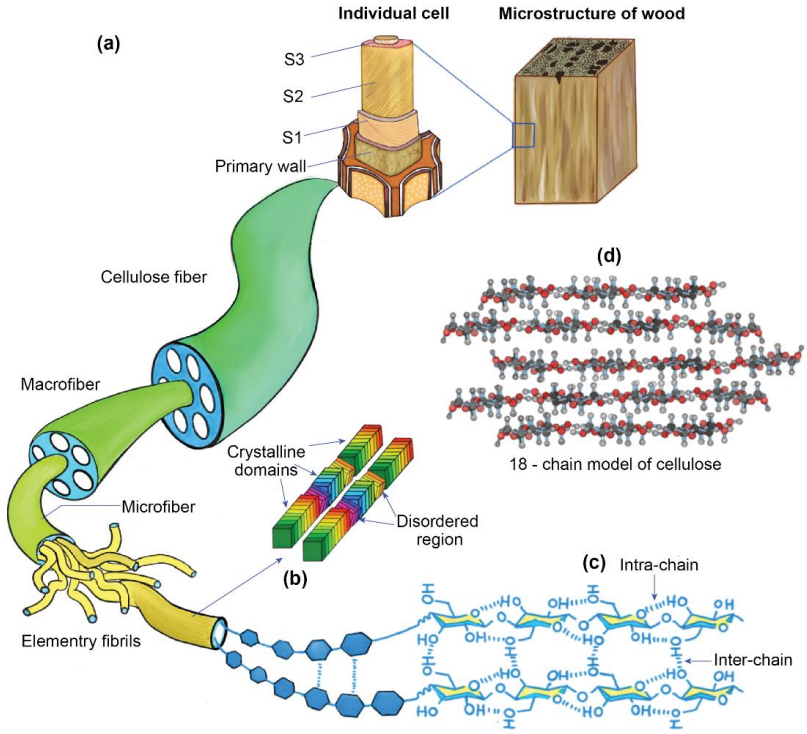

Figure 2. The hierarchical structure of plant cell walls showing: (a) plant cell wall of wood; (b) elementary fibril crystalline and disordered regions; (c) cellulose chains at a molecular level; (d) the 18-chain model. (Inspired from ref.[27,53])

Cellulose microfibrils continue to draw attention in academia and industries to untap their potential as a green, renewable and sustainable material. The presence of these cellulose microfibrils in the plant cell wall plays a pivotal role in fiber reinforcement and is responsible for maintaining the shape and rigidity of plant cells,[54] whereas lignin and hemicellulose in the vicinity serve as a matrix (Figure 2a) [55]. The isolation of these individual cellulose microfibrils from the cell wall is challenging[51] due to the compact hierarchical structure of the plant cell wall and the aggregation tendency of cellulose. Therefore, to preserve the nanoscale dimensions and the long axial length of CNF it is important for the extraction process to be precise.

Mechanical fibrillation is the most common isolation method to obtain cellulose nanofibrils, which can produce CNF with a diameter range of 5-20 nm.[47] The length of the CNF fibrils is hard to determine and may exceed 5 μm.[47] To reduce energy consumption and to obtain CNF with specific properties, pretreatment such as TEMPO-oxidation is often employed. The addition of the charge on the surface of microfibrils promotes the fibrillation process, resulting in highly monodisperse CNF widths of 3–4 nm.[56] Several other pretreatments, such as acid hydrolysis[57], enzymatic treatment [58,59], and carboxymethylation [60] are often employed to ease the fibrillation process. Here, it is important to mention that there are different terminologies used in literature for mechanically

fibrillated microfibrillar cellulose such as microfibrillated cellulose (MFC), nanofibrillated cellulose (NFC), cellulose nanofibrils (CNF), and nanocellulose. To follow Tappi standards, the term "CNF" will be used hereafter.

The properties of the CNF obtained, such as morphology, size, and surface features largely depend on the cellulose origin, the fibrillation process, and any pre-treatment or post-treatment. The most promising attributes associated with CNF apart from its renewability and biodegradability include high surface area (150–600 $m^2\ g^{-1}$), high aspect ratio (~1000), excellent mechanical properties (strength of 1-3 GPa and crystal modulus of 138 GPa), low coefficient of thermal expansion (0.01 $ppm \cdot K^{-1}$) and low density.[61] This unique set of properties of CNF are immensely attractive for large-scale industrial applications as a replacement to synthetic plastics, especially for nanocomposites, packaging, aerogels, etc. However, besides enticing features, CNF has some challenges which hinder its applications at a large commercial scale.

3.3 Lignin: From raw lignin to colloidal lignin nanoparticles

Lignin is the second major contributor to lignocellulosic biomass. The presence of lignin in the plant cell wall is crucial for its survival and development.[62] In the form of a linear oligomer, [32–34] lignin surrounds the cellulose and hemicellulose as a protective constituent.[63] The lignification of the cell wall of aquatic plants was imperative for their survival in a terrestrial environment by providing structural rigidity, hydrophobicity, water permeability control, UV-protection, and anti-microbial properties.[64] Lignin is a heterogeneous complex polymer formed by the radical coupling polymerization of three primary monolignols: *p*-coumaryl, coniferyl, and sinapyl alcohols, as drawn in Figure 3. A variety of groups which include hydroxyl, carbonyl, methoxy, and carboxyl groups directly affect the reactivity of lignin in different chemical reactions.[65,66]

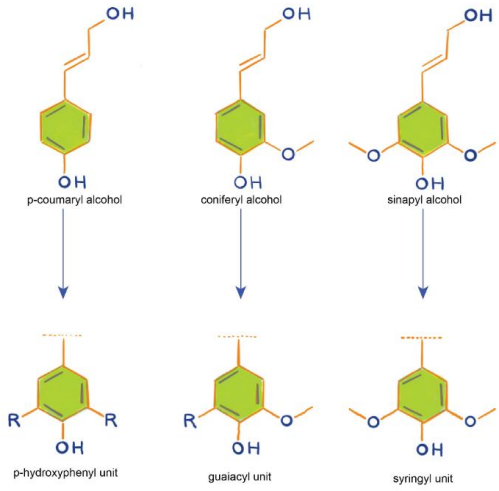

Figure 3. Lignin precursors and their corresponding structural units. (Adapted from ref.[23])

Lignin is produced in high volumes as a side stream by the pulping and biofuel industry.[67] From a sustainability point of view, it is highly desirable to benefit from the molecular structure of lignin to produce a variety of value-added materials. However, its relatively recalcitrant nature and the high complexity of the lignin structure hampered its conversion to specialty applications.[23,68] For decades, various strategies such as thermal, catalytic, and biological treatments have been employed to obtain monomeric constituents for lignin valorization.[69] However, inherent heterogeneity also prevails at the monomeric level, resulting in aromatic species of diverse nature, which are unacceptable for high purity chemicals production.[69]

Considering these limitations posed by the chemical nature of lignin, a distinctive path towards its utilization was necessary. In this regard, the emergence of colloidal lignin particles, also called lignin nanoparticles (LNPs) have presented a remarkable opportunity.[23] In recent years, various methods for the preparation of lignin nanoparticles including solvent shifting [70–74], acidification[75–77], CO_2 precipitation[78], aerosol-flow[79] (Figure 4b), and reverse micelle formation[80] have been reported. In brief, during the dissolution of lignin in a solvent-water binary mixture, the hydrophilic functional groups (phenolic and aliphatic hydroxyl groups) interact with water molecules and the hydrophobic moieties (phenylpropanoid units) shows a tendency towards organic solvent. The introduction of anti-solvent (water) reduces the ratio of organic solvent within the system, hence provoking the self-assembly of lignin into spherical lignin nanoparticles.[23,81,82] During the process of self-assembly, lignin chains reconfigure and attain a favorable conformation, where higher molecular weight lignin chains construct the nuclei and lower molecular weight lignin chains form the outer surface. The resulting lignin nanoparticles have surfaces rich in –OH and –COOH functional groups [81,82] which provide extensive possibilities for tailoring the surface properties for diverse applications.

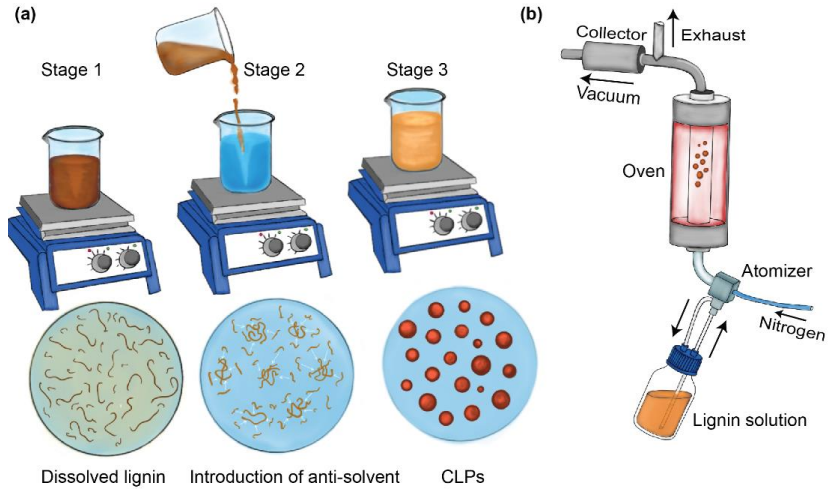

Figure 4. Preparation of CLPs; (a) stages of solvent-the exchange method and (b) aerosol-flow reactor setup. [79]

Among the various lignin nanoparticle fabrication methods (Table 1), solvent shifting/solvent exchange is a frequently used method. Lignin nanoparticles obtained from this method exhibit spherical geometry and a narrow size distribution.[23] By adjusting certain variables, such as initial lignin concentration, pH, choice of the solvent, and molecular weight (Mw) of lignin, the size of the nanoparticles can be fine-tuned.[23] Furthermore, the fabrication process is simple, cost-effective, and has scaling-up opportunities as shown in Figure 4a. In contrast, the lignin nanoparticles prepared by rapidly adding acid into the aqueous lignin solutions, often referred to as acid precipitation, leads to the formation of irregular clusters of lignin particles. The presence of residual acid in the final product and pH-dependence are further drawbacks of the acid precipitation method. Therefore, in our work, we utilized colloidal lignin particles from the solvent exchange method to benefit from the spherical geometry and large surface area of the CLPs obtained for nanocomposite applications. A few examples of different methods utilized to prepare nanoparticles from different lignin sources and solvent systems are tabulated in Table 1.

Table 1. Examples of the various lignin nanoparticle production methods[23]

Preparation Method	Lignin type	Solvent	Antisolvent	Ref.
Solvent shifting	AL, KL,	THF	H_2O	[70] [73] [72]
	KL	THF/H_2O	H_2O	[74]
	KL	Acetone/ H_2O	H_2O	[83]
Acidification	KL	EG	HCl	[84]
	KL	EG	HNO_3	[75]
Aerosol flow reactor	KL	DMF	None	[79]
	KL	DMF		[85]
Sonication	AL	H_2O		[86]
CO2 precipitation	KL	DMF	CO_2	[78]

THF = tetrahydrofuran, DMF = N,N-dimethylformamide, EG = ethyleneglycol, KL = kraft lignin, AL = alkali lignin.

The formation of homogeneous spherical nanoparticles from crude lignin circumvents the limitations of its structural complexity and offers a wide range of potential applications, such as active drug carriers, nanocomposites, UV shielding, and antioxidant agents.[23]

3.4 Bio-inspired nanocomposites

Strong emphasis on environmentally friendly materials has created a fascinating interdisciplinary field where material science and biology meet nanotechnology. The outcome of this unique merger forms the basis for bio-nanocomposites, which aims to utilize materials from nature at nanoscale morphology to attain superior properties. The bio-based component imparts biocompatibility and biodegradability, whereas the nano-component, due to its large surface area, enhances the interaction between the reinforcement and matrix resulting in high strength and improved properties.[87] A variety of biomaterials exists in nature such as polysaccharides, polypeptides, and proteins. However, this thesis is focused on lignocellulosic biopolymers, mainly cellulose and lignin in the form of CNF and CLPs respectively.

3.5 CNF and CLPs based bionanocomposites

Since the cellulose nanofibrils act as a load-bearing component in the plant cell wall, their use as a reinforcement in nanocomposites is not surprising. The strength of 1-3 GPa and crystal modulus of 138 GPa, combined with low density have validated their use in composite papers and films in diverse applications such as packaging, biomedical, energy, and flexible electronics.[47,54,88] Different biopolymers such as poly (lactic acid), polycaprolactone, starch, chitosan, amylopectin, and gelatins have been combined with CNF to prepare nanocomposites.[61]

CNF based nanocomposite films also referred to as "nanopaper", are often prepared by filtering a CNF suspension of 0.2 – 0.8 wt %. The large number of OH groups present on the surface of nanofibrils and secondary interactions cause the cellulose chain to form an entangled network structure upon the removal of water. The presence of hydroxyl groups on the CNF surface plays a crucial role while preparing the nanocomposite. The interactions between the reinforcement (CNF) and matrix (biopolymer) and their compatibility are key to forming a strong nanocomposite film.[89] Therefore, CNF is more evenly dispersed in hydrophilic polymer matrixes and form highly strong nanocomposites. However, this hydrophilicity becomes a severe disadvantage when dispersing CNF in non-polar hydrophobic polymer matrices.[89] To extend their use in nonpolar environments, several surface treatments have been proposed to increase the compatibility of CNFs with hydrophobic systems.[90] However, chemical modification disrupts the hydrogen bonding network leading to poor mechanical properties.[91] Furthermore, the structural changes in CNF in response to these treatments hampers its biodegradability and is detrimental to its inherent properties.[92]

In contrast to cellulose, lignin has mainly been used in low-demand applications such as heating and energy generation. However, the reconsideration of lignin and its side-streams as a platform for a variety of chemicals and materials have brought it into the spotlight again. From the standpoint of harnessing the multifunctionality of lignin such as an antioxidant, antimicrobial, UV-shielding, and reinforcing filler, nanocomposites provide a fitting route. It is anticipated that the large surface area and active surface sites will facilitate the interaction between CLPs and the polymer matrix, resulting in better dispersion to form strong nanocomposites.[93]

Until now most of the work regarding utilization of lignin for nanocomposites relied on the use of lignin microparticle ranging from (10-100μm) with little to no beneficial improvements.[94] Certain chemical modifications such as nitration, esterification, and salinization have also been practiced, increasing the compatibility of lignin with polymeric and biopolymeric systems.[95] But the breakthrough came with the introduction of nanolignin in the form of colloidal lignin particles. The large surface area and well-defined surface chemistry of CLPs are anticipated to improve its dispersion and enhance matrix-to-nanofiller interaction at the interface, paving the way for developing sustainable bio-nanocomposites. [93]

In a short period, a multitude of composites has been prepared by utilizing the multifunctional attributes of CLPs for reinforcing CNF, proteins, natural rubber, and a variety of biopolymers such as Polyvinyl alcohol (PVA), chitosan, and PLA.[96] The hydrophilic nature of CLPs has made them possible to disperse in water-based systems, however, their use in the hydrophobic system requires further exploration. An overview of the main recent nanocomposite applications of CLPs, with respect to the diameters of lignin nanoparticles, used biopolymer, and property improvements are depicted in Table 2.

Table 2. Use of CLPs in nanocomposites, with reference to the lignin particle diameter, biopolymer matrix used and major findings

CLPs Diameter	Biopolymer	Property enhancement	Ref.
295 nm	PVA	Improvement in tensile strength, antioxidant, and UV shielding properties	[93]
224nm	PVA	Improvement in the water vapor barrier, UV-shielding, and mechanical properties	[97]
10-20 nm	PVA	UV-shielding efficacy	[98]
40-60nm	wheat gluten	Mechanical performance, thermal stability, and UV resistance improvement	[99]
40-60nm	CNC, PLA	Improvement in mechanical properties, optical and thermal properties	[100]
na	PVA, Chitosan	Improvements in the mechanical performance, thermal stability, antioxidant and antimicrobial	[96]

CLPs have been successfully employed in a combination of water-based biopolymer systems to improve mechanical, thermal, antioxidant, and UV-shielding properties. The enriched functional groups present at the CLPs surface give rise to strong interfacial adhesion leading to the improvement in nanocomposite properties. The intrinsic properties of CLPs not only make them suitable for nanocomposites but the presence of easily tuneable functional groups on their surfaces increases their potential for a wide range of biomedical applications and active substance carriers, as will be discussed in the following chapter.

3.6 CLPs as vehicles for active substances

The conversation of crude lignin, with very limited and mainly low-value uses, to CLPs with such a wide range of applications has unlocked a broad range of opportunities. The unique surface features of CLPs acquired through the self-assembly process, such as spherical morphology, well-defined surface chemistry, large surface area, and negative charge, have advanced CLPs as a versatile material.[23,101] Apart from their use in nanocomposites to avail their multifunctionality, another high-end use of CLPs as vehicles to deliver different biological or therapeutic compounds is progressing rapidly.[77] A variety of methods, such as adsorption, entrapment, encapsulation, and covalent bonding have already been practiced successfully to load active substances into or upon CLPs (Table 3).[23] The flexibility of CLPs based carriers relies on the fact that active substances can be loaded before, during, or post nanoparticle formation. Furthermore, CLPs offer the possibility of entrapping an active substance within the core of CLP and adsorption of another active substance on the surface of CLP, which is highly desirable for targeted applications. In the presented work, CLPs

are utilized as low-cost enzyme carriers for aqueous ester synthesis by the adsorption and entrapment method (Paper V).

Table 3. Use of CLPs as an active ingredient, with reference to the lignin source, particle preparation method, particle diameter, active substance, and target application

Lignin source	CLPs Preparation method	CLPs Diameter (nm)	Active substance	Target	Ref.
AL	Solvent shifting	131 - 179	Resveratrol	Anticancer effects	102
KL	Solvent shifting	160 - 221	Sorafenib and benzazulene	Drug loading and release efficiency	103
OS	Ultrasoniation	104	Curcumin	Lipophilic drug model	104
AL	Solvent shifting	100 ~ 400	Ibuprofen	pH-responsive release	105
KL	Ultrasonication	200 – 300	Fungicides	Fungal grapevine trunk disease Esca	106
KL	Solvent shifting	122 - 190	tall oil fatty acid, oleic acid, or lauric acid	Thermally responsive phase-change materials.	107
SL	nanoprecipitation Solvent shifting	312 - 67	Budesonide	pH-triggered and surfactant-responsive release of corticosteroid	77
KL	Solvent shifting	215	Glucose oxidase chitosan	Pickering emulsion polymerization stabilizers	101
KL	Solvent shifting	177	Lipase M	Biocatalytic ester synthesis in aqueous media	108

SL = soda lignin, KL = kraft lignin, AL = alkali lignin, OS = Organosolv

3.7 CNF based aerogels

Aerogels are interconnected, three-dimensional (3D) porous materials obtained by replacing the liquid with air, without significantly varying the network structure along with minimum shrinkage during the solvent removal process.

CNF aerogels are characterized by low density (higher than 99% porosity), and a high specific surface area.[109,110] The volume of the solid phase in the CNF network is only in the range of 0.2 to 20% of the total volume. The procedure of preparing CNF based aerogels involves gelation and drying. In general, freeze-drying is a widely explored route to prepare porous CNF aerogels, although solvent exchange, vacuum drying, supercritical CO_2, and some other techniques have also been employed.[109]Even though CNF aerogels are not prepared through the classical route of sol-gel and often contain large micron-sized pores, the term “cellulose aerogel” has been still widely accepted among researchers. Due to its extremely low density, ultrahigh surface area and low thermal conductivity, low thermal expansion, biocompatibility, and sustainability, CNF aerogels offer a wide range of potential applications ranging from nanocomposites, biomedicine, insulation to absorbents.[109,110] Among other applications, thermal insulation is well-suited for CNF materials, however, they lack flame-retardancy, which needs to be addressed.

3.8 Flame retardant CNF based aerogels

The thermal conductivities exhibited by CNF based aerogels is below 25 mW m^{-1} K^{-1}, which makes them suitable candidate as building insulation materials.

However, the very high flammability of CNF aerogels inhibits their use for building insulations. Since CNF is readily flammable its hybridization with fire-resistant materials is necessary. Most of the flame retardants commercially available are either oil-based or halogenated, organophosphorus-based compounds, which present serious health risks and detrimental environmental effects.[111] Thus, there is a need to develop bio-based insulation materials with eco-friendly flame retardancy. Various flame retarding materials have been incorporated in CNF aerogels to improve their flame retardancy and a few examples are listed in Table 4. In the presented work (Publication I) CNF aerogels were prepared by integrating sodium bicarbonate that efficiently enhances the fire retardancy.

Table 4. Examples of CNF based flame-retardant aerogels

Flame retardant	Thermal conductivity ($mW\ m^{-1}\ K^{-1}$)	Ref.
N-methylol dimethylphosphonopropionamide , 1,2,3,4-butanetetracarboxylic acid	32.58	[112]
Hydroxyapatite (HAP)	38.5 – 39.1	[113]
MgAl-layered double hydroxide	37.1	[114]
Sodium montmorillonite (MMT), boric acid (BA), and melamine-formaldehyde (MF)	30-35	[115]
Sodium bicarbonate (SBC)	28	[116]

4. Experimental

In this chapter, the materials and methods used in this thesis work are described. The "Material" section contains the information concerning the primary raw materials and their processing, whereas the "Methods" section covers the important characterization techniques used for the investigation of scientific phenomenon. A detailed description of the materials, instrumentation and methods used in this thesis can be found in the materials and methods section of each original Publication (I–V).

4.1 Materials

4.1.1 Cellulose nanofibrils (Publications I & III)

Hardwood kraft pulp was utilized as the starting material for the preparation of CNF used in Publications I and III. Before fibrillation, the earlier reported[117] washing procedure was commenced in the following way. Pulp was first washed with 10^{-2} M HCl and subsequently with deionized water. The conversion of carboxyl groups to their Na-form was proceeded by treating the pulp fibers with 10^{-3} M SBC and the addition of NaOH to reach pH 9. Afterward, the excess electrolyte was removed with deionized water. Fibrillation of the pulp fibers commenced using a high-pressure microfluidizer (Microfluidics, M-110Y, Microfluidics Int. Co., Newton, MA). The pulp was once passed through the fluidizer with 400 and 200 μm chambers and 6 times through the 400 and 100 μm chambers at 2000 bar of pressure.

The CNF suspension used in Publication IV was prepared using Masuko Supermasscolloider (MKCA6-2 J CE; Masuko Sangyo, Japan). Softwood sulfite pulp at 1.6 wt % consistency was passed through the grinder multiple times at different disk gaps, which are one pass at zero micrometer disk gap, three passes through -20 μm, four passes through −40 μm, five passes through −60 μm, and seven passes through −90 μm.

4.1.2 Lignin (Publication II, III and V)

Softwood kraft lignin BioPiva™ 100 acquired from UPM Biochemicals, Finland was utilized for all the work presented involving lignin.

Preparation of kraft lignin suspension
The kraft lignin suspension utilized in Publication III was prepared by suspending a predetermined concentration of kraft lignin in deionized water, followed by homogenization using an IKA T18 basic ULTRA-TURRAX device at speed 5 for 1 min.

Preparation of water-soluble cationic lignin (Catlig)
The synthesis of water-soluble cationic lignin commenced by dissolving a known amount of lignin in 0.2M sodium hydroxide, followed by the drop-wise addition of glycidyl trimethylammonium chloride to start the 1 h reaction at 70 °C. After the completion of the reaction, purification of the reaction products was carried out by dialysis at pH 7 in Spectra/Por® 7 tubing with an MWCO of 1 kDa (Spectrum Labs) against deionized water for 4 days. Afterward, yields were calculated based on the initial lignin dry weight. Cationic lignin utilized for Publication III originated from the same batch as described by Sipponen et al.,[118] whereas, for Publication II and IV, separate individual batches were synthesized following the same procedure outlined above, adopted from earlier reported work. [118]

Preparation of colloidal lignin particles (CLPs)
All the CLPs used were prepared using the solvent exchange method, as described previously. [118] In the first step, 5.00 g of softwood kraft lignin (dry basis) was dissolved in 500 mL of an acetone/water (3:1, v/v) binary mixture. Stirring was sustained for 3 hours, followed by filtration to remove undissolved lignin fragments using a glass microfiber filter (Whatman GF/F, pore size 0.7 μm). The solvent exchange was executed by rapidly pouring the filtered lignin solution into 1000 g of deionized water vigorously stirred. Removal of acetone was conducted using rotavapor at 40° C under reduced pressure. For Publication II, CLPs were prepared using two different solvent systems, THF–water and acetone–water binary mixtures, but otherwise following the same procedure described above.

Preparation of cationic-colloidal lignin particles (c-CLPs)
Preparation of c-CLPs was carried out by adopting an earlier reported procedure.[118] In brief, a CLP dispersion was mixed with an aqueous cationic lignin (Catlig) solution at pH 4 under vigorous stirring. By changing the Catlig to CLPs dry weight ratios, 5 different c-CLPs at 50, 100, 150, 200, and 300 mg g^{-1} were also obtained (Publication III).

4.1.3 Sodium bicarbonate (SBC) (Publication I)

SBC, a white crystalline powder is a monosodium salt of carbonic acid. Commonly, SBS is used as a pH buffering agent, system alkalizer, a blowing agent, and in most dry fire extinguishers. The SBC used in this work (Publication I) was acquired from ICN Biomedicals Inc. (Ohio).

4.1.4 Poly-L-lysine (PLL) (Publication II)

Poly-L-lysine is a typical cationic polypeptide, which is fully charged at low pH and adopts an extended coil conformation, whereas in the pH region 9–11 it deprotonates and adopts a β-sheet structure.[119] PLL readily adsorb onto a variety of negatively charged surfaces like metals, polymers, and glass, via electrostatic interactions due to the presence of the positively charged lysine amine groups on PLL.[119] Therefore, in our work (Publication II) PLL, acquired from Sigma-Aldrich at a concentration of 0.1% (w/v) and a molecular weight (M_w) of 150,000–300,000 g mol^{-1} was employed as an anchoring polymer.

4.1.5 Polystyrene (PS) (Publication II)

For the preparation of model surfaces from dissolved lignin in Publication II, PS having a Mw of 280,000 g mol^{-1} was acquired from Sigma-Aldrich and was used as anchoring polymer on gold and silica substrates.

4.1.6 L-(+)-Lactic acid (80%) and water-based polyurethane (PU) (Publication IV)

L-(+)-Lactic acid (80%) and the anionic surfactant-based polyurethane dispersion (UH240) utilized in this work (Publication IV) were purchased from Sigma-Aldrich.

4.1.7 Enzymes (Publication V)

Lipase M from *Mucor javanicus* and *Humicola insolens* cutinase (HiC) were acquired from Novozymes, China.

4.2 Methods

4.2.1 Preparation of flame-retardant CNF aerogels (Publication I)

The freeze-drying method was employed for preparing CNF based flame retardant aerogels. In the first step, mixing of CNF suspension (0.5 wt%) with sodium bicarbonate at four different weight percentages (10, 20, 30, and 40%) was carried out. To ensure the homogeneous dispersion of SBC in CNF, an IKA ULTRA-TURRAX disperser was used at 10 000 rpm for 10 min. During the second step, the mixture was placed in a heating oven for 60 min at 100°C followed by freeze-drying. A schematic illustration of the fabrication procedure is presented in Figure 5.

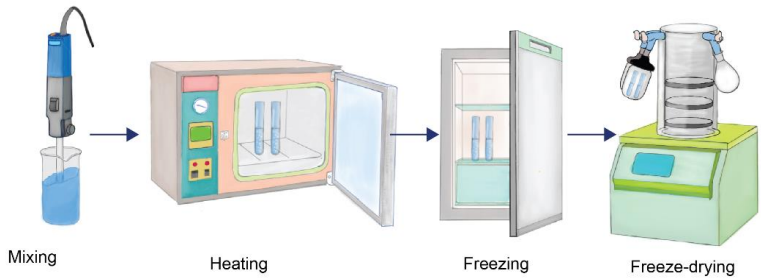

Figure 5. Schematics of the flame-retardant aerogel fabrication procedure. **(Publication I)**

4.2.2 Thin films preparation (Publication II)

Model surfaces from CLPs on silica and gold substrates were prepared by two commonly employed methods: spin coating and adsorption. In the case of spin coating, silica wafers of 1.5 cm × 1.5 cm dimensions were submerged in 1 M NaOH solution for 15 s, followed by rinsing with Milli-Q water and dried under nitrogen. In the next step, silica wafers were treated with UV/ozone for 15 min. The spin coating procedure commenced by first applying an anchoring layer of PLL onto the silica substrate at 2000 rpm for 90 s, then the CLP layer was deposited using the same parameters. For two-deposition thin films, another layer of CLPs was deposited under the same conditions. Rinsing and nitrogen drying was practiced between each step.

For the adsorption method, CLP thin films at longer adsorption times (12 h for PLL and 12 h CLPs) and shorter adsorption times (30 min for PLL and 60 min CLPs) were prepared. PLL was first adsorbed by immersing the treated silica or gold substrates into PLL solution. After the successful adsorption of PLL, CLPs were adsorbed using the same procedure. The process was repeated for two-deposition thin films.

Three different concentrations of CLPs, 0.5, 1.0, and 1.5 g L^{-1}, were utilized to prepare CLP thin films from both spin coating and adsorption methods. The illustration of the thin film preparation is presented in Figure 6, and for the detailed information, Publication II is referred to.

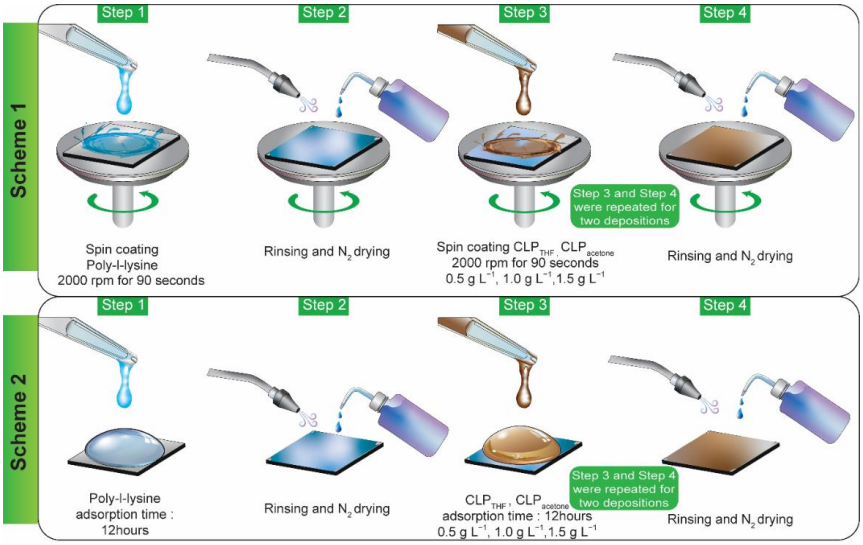

Figure 6. Schematic illustration of thin-film preparation from spin coating scheme 1, and adsorption process scheme 2. **(Publication II)**

4.2.3 CNF based nanocomposite films preparation

For the preparation of pure CNF and nanocomposite films, the filtration method was adopted with slight modifications.[47] The first step involved the dilution of a CNF suspension to 0,8 wt % followed by stirring for 2 hours in the case of pure CNF films. For lignin-containing nanocomposite films, after 2hrs of magnetic stirring of the CNF suspension, the lignin suspension was added and the mixture was mixed for 15 min. Filtration started at 2.5 bar overpressure for 45 minutes through a 10 µm pore size open mesh Sefar Nitex polyamine monofilament fabric which was placed on the top of a VWR grade 415 filter paper. After filtration, filtrates were collected to calculate the mass balance. For ambient dried samples, wet films were sandwiched between blotting papers and kept at 23 °C and 50% relative humidity (RH) for 72 h under a load of 5 kg. To prepare hot-pressed films, a Carver Laboratory press (Fred S. Carver Inc.) was used at 100 °C and 1800 Pa for 90 min.

On the other hand, for preparing pure CNF and CNF-PU nanocomposite films, a filtration method with different parameters was employed. Firstly, a CNF suspension was diluted to a concentration of 0.2 wt % and then UH240 was added to the CNF suspension along with lactic acid equal to the amount of CNF dry content, to facilitate the draining of water during filtration. The mixture was homogenized using a high-speed ultraturrax at 10,000 rpm followed by sonication until the energy imparted was 300 J ml^{-1}. Filtration proceeded over a Durapore PVDF membrane filter (Fisher Scientific, Pittsburgh, USA) with a pore size of 0.65 µm at 70 ± 5 kPa. Hot pressing of the wet films was conducted at 100 °C at a pressure of 5 MPa for 30 min.

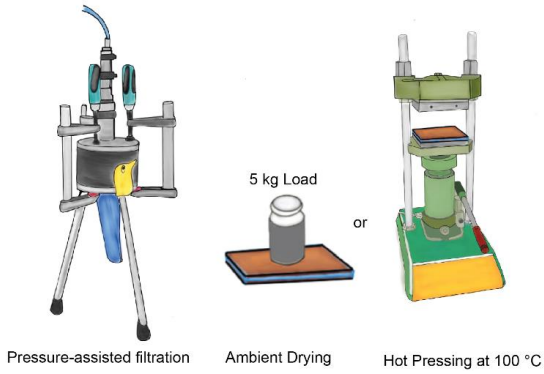

Figure 7. Schematic illustration of nanocomposite film preparation. **(Publication III)**

4.2.4 Enzyme immobilization on CLPs (Publication V)

The preparation of CLPs as enzyme carriers proceeded in the following way. During the first step, prepared CLP were coated with cationic lignin 9% (w w^{-1}) by adsorption. The second step involved the adsorption of hydrolases onto the cationic lignin nanoparticles. This step was repeated to ensure a homogenous surface coverage for 15 min at 22 °C each time. Afterward, coated particles were mixed with aqueous sodium alginate, followed by dropwise precipitation in 0.2 M aqueous calcium chloride at room temperature. Washing and drying at ambient conditions were carried out to obtain enzyme immobilized beads.

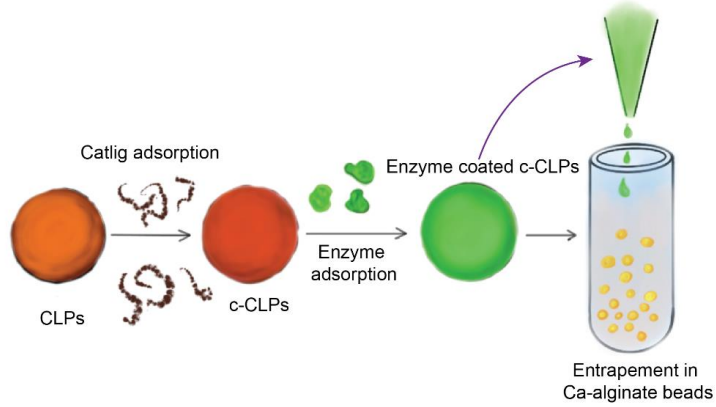

Figure 8. Schematic illustration of the enzyme immobilization process. **(Publication V)**

4.3 Morphological characterization

4.3.1 Atomic force microscopy (AFM)

The atomic force microscope also referred to as scanning force microscope is one of the scanning probe microscopes. The underlying principle of AFM is that a tip is attached at the end of a flexible cantilever that interacts with the sample, which deflects in response to the attractive or repulsive forces. Laser light focused at the end of the cantilever is reflected and subsequently detected by a

quadrant photodiode. The images are formed by recording the interactions between the surface and the tip. There are three primary modes of AFM, known as contact mode, tapping mode, and non-contact mode. In contact mode, the tip is continuously in contact with the sample surface, which is preferably used only with hard surfaces. In the case of intermittent or tapping mode, the AFM tip oscillates over the sample surface. The tapping mode is more suitable for biological samples. In non-contact mode, the tip vibrates close to its resonant frequency in the proximity of the surface and never comes in contact with the sample.

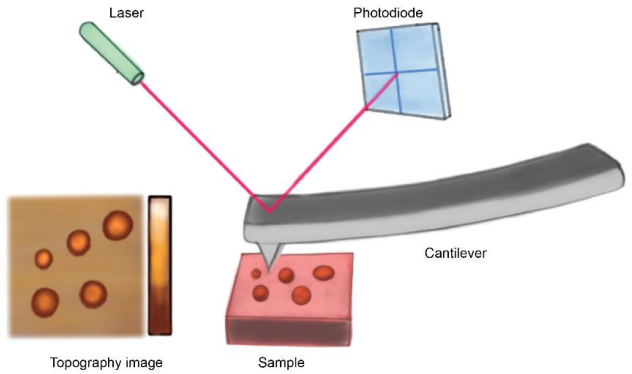

Figure 9. Typical AFM setup representation.

For Publication II, a MultiMode 8 atomic force microscope equipped with a NanoScope V controller (Bruker, Santa Barbara, CA) was utilized to obtain high-resolution topographical images of the lignin thin films in tapping mode. Images were processed using NanoScope Analysis 1.5 or NanoScope 8.15 softwares (Bruker).

4.3.2 Field Emission Scanning Electron Microscopy (FESEM)

To obtain morphological information of the flame-retardant aerogels, nanocomposites films, and CLPs, different field emission scanning electron microscopes were used. In all cases, the sample surfaces were sputter-coated either with gold/palladium or platinum. Images were captured at acceleration voltages of 1.5 to 5 kV, using an in-line secondary electron detector. Detailed information can be accessed from the original Publications.

4.3.3 X-ray microtomography (MicroCT)

A non-destructive X-ray microtomography technique was employed to gain comprehensive morphological information of the flame-retardant aerogels prepared in Publication I. The MicroCT working principle is based on X-ray radiography, where the change in x-ray absorbance observed in a given sample causes a contrast. By taking several radiographs at different viewing angles, a 3D map is generated providing detailed structural information of a volume. In

our work (Publication I), a Bruker SkyScan 1272 (Kontich, Belgium) at a source voltage of 30 kV, a current of 212 µA, and a pixel size of 14.998 µm was utilized to analyze 10 x10 mm (diameter, length) aerogel samples. A total of 550 projections were recorded for each sample.

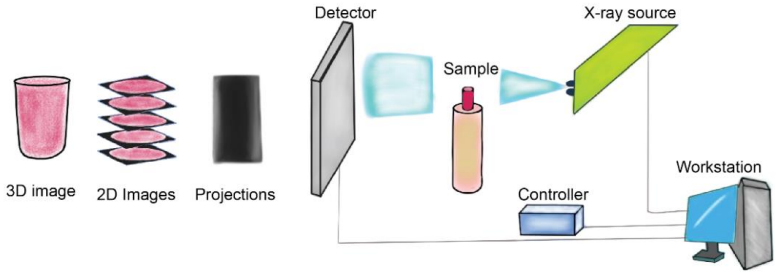

Figure 10. X-ray MicroCT equipment configuration.

4.4 Contact angle measurements

Contact angle measurement is an essential tool to study the wettability of a surface due to its simplicity and versatility. Most commonly, an optical-based sessile drop method is used for measuring the contact angle. A typical goniometer setup consists of a horizontal sample mounting station, located between the light source and a CCD camera. A mechanized dispensing unit dispenses a specific volume of desired liquid onto the test sample surface, forming a sessile drop. To obtain the contact angle values, curve fitting of the liquid drop profile is employed using a built-in software.

For Publication II, a fully automated theta flex optical tensiometer from Biolin Scientific (Gothenburg, Sweden) was employed to determining the static WCAs of the different lignin and pure PLL substrates. To elucidate the effect of humidity on contact angle values, conditioning of the samples was performed at 15% RH and 50% RH at 23 °C for 48 h before the measurements. For Publication IV, The static contact angles of Milli-Q water droplets on pure CNF and PU-CNF nanocomposite films were measured at room temperature using a CAM 200 (KSV Instruments Ltd, Helsinki, Finland).

Measurements were executed by placing a ~ 6.5 µL drop of Milli-Q water on both sides of the films using a dispensing unit. Images were captured at the rate of one frame per second, sent directly to the computer for analysis via the CCD camera. Software provided by the instrument manufacturer was utilized to compute the static contact angle values based on the Young-Laplace equation.[120]

4.5 Mechanical testing

CNF based nanocomposites are particularly attractive as lightweight structural materials; therefore, their mechanical properties are of considerable interest. Tensile testing is regularly applied to obtain different mechanical properties, such as tensile modulus, yield strength, tensile strength, elongation at break, and toughness of CNF nanocomposites. In Publication III and IV, the universal testing machines Instron 4204, (U.S.A), and Instron 5544 (Norwood, USA) both

equipped with a 100 N load cell was used, respectively. Rectangular specimens of 50 × 5 mm² were first conditioned at 50% RH for 48 hours and subjected to a 2 mm min⁻¹ strain rate. Measurements were performed in a controlled environment of 50% RH at 23 °C.

4.6 Quartz crystal microbalance with dissipation monitoring

Quartz Crystal Microbalance with Dissipation monitoring (QCM-D) is one of the surface-sensitive tools for real-time monitoring of surface interaction phenomena, the formation of thin films, and the properties of the adsorbed layer.

In principle, QCM-D is a nano-balance, measuring a mass per unit area by detecting the frequency change (Δf) of the quartz crystal resonator. A typical QCM-D setup consists of a megahertz piezoelectric quartz crystal with electrodes deposited on both sides, an oscillator to run the crystal, a flow module, and electrical connections. When, the quartz crystal, oscillating at its resonant frequency, is subjected to adsorption of additional mass, a frequency change (Δf) occurs, allowing the detection of adsorbed mass. Figure 11 provides illustrative details of the experimental setup and measurement principle.

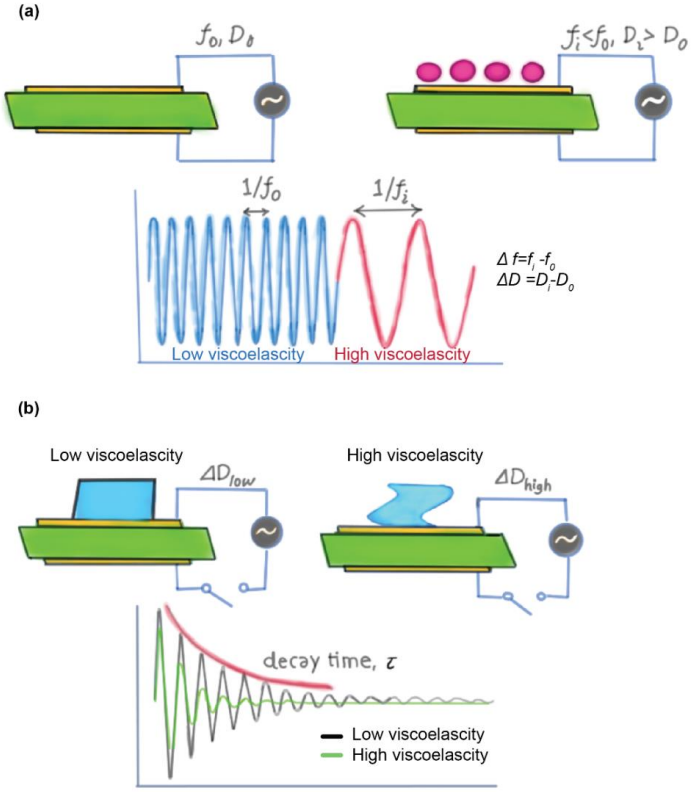

Figure 11. Schematic illustration of QCM-D measurement principle; (a) change in frequency and dissipation before and after adsorption; (b) dissipation factor for rigid and viscoelastic layers.

QCM-D can measure both frequency and dissipation responses of the quartz crystal. The dissipation indicates how fast the oscillatory energy of the crystal

dissipates when the driving voltage is switched off. The dissipation factor gives information regarding the nature of adsorbed layer onto the QCM-D sensor surface. Energy dissipation (Δ D) is proportional to $1/\tau$, where τ is the decay time constant. The Δ D of a rigidly adsorbed layer, attached to the surface will be smaller compare to a viscous layer because the ratio of energy loss and energy stored is smaller for rigid layers compared to soft and viscous layers. In our experimentations, we utilized the QCM-D E4 (Q-Sense, Gothenburg, Sweden) to monitor the *in-situ* adsorption of CLPs onto PLL-coated QCM-D sensors along with the evaluation of their swelling and stability and adsorption of Catlig.

4.7 Thermal analysis

Thermal analysis is a collection of valuable tools to investigate the change in material properties with respect to a change in temperature. By analyzing a bulk sample of few milligrams, detailed information of a nanocomposite system and the effect of different components such as filler on thermal properties can be obtained. In Publication I, a thermogravimetric analyzer (TA Instruments Q500) was employed to obtain the thermal properties of the pure and flame-retardant CNF based aerogels. Aerogel samples were heated under a nitrogen atmosphere from 25 to 600 °C at a heating rate of 10 °C min^{-1}. To measure the thermal conductivities (λ) of the flame-retardant aerogels, a C-Therm thermal conductivity analyzer (C-Therm TCi) with a modified transient source plane technique was employed. Three cylindrical samples (diameter ~ 25 mm, height ~ 7 mm) of each aerogel were measured at 24 °C from the top and bottom surfaces. Whereas, for the evaluation of the flame-retardancy performance of modified aerogels, a horizontal combustion test was utilized.

4.8 Dynamic vapor sorption (DVS)

A dynamic gravimetric water sorption analyzer (DVS Intrinsic, UK) was used to investigate the water sorption capacity of CNF-based nanofilms. A sample of up to 15 mg was placed in the sample pan and then weighed with a resolution of 0.1 µg. The measurements were made at 25 °C. The RH was set to increase from 0% to 95% in 20 steps and then decrease to 0%. At every target humidity stage, the RH was kept constant until the rate of sample mass change was less than 0.001% min^{-1}, before proceeding to the next increment. The following equation was utilized to calculate the moisture uptake of each sample:

$$\text{moisture uptake } = 100 \times \frac{W_{moist} - W_{dry}}{W_{dry}}$$

where, W_{moist} is the weight of the sample equilibrated at a certain RH% and W_{dry} is the dry sample weight at 0 RH%.

4.9 Differential scanning calorimetry thermoporometry (tp-DSC)

The porous nature of the pure CNF and lignin CNF nanocomposite films was evaluated by using tp-DSC adapted from Park et al.,[121] and using the published

temperature program.[122] Thermoporometry is based on the freezing point depression of water confined in pores, with the melting point increasing as the pore diameter increases. For tp-DSC, circular samples were submerged overnight in deionized water for complete wetting. Wetted samples were placed in 50 µL pre-weighed aluminum pans and were sealed using a pan crimper press. Duplicate measurements were carried out on a DSC 6000 (Perkin Elmer, USA) equipped with a cooling apparatus under a nitrogen gas flow rate of 20 mL min^{-1}.

5. Results and Discussion

In this chapter, the utilization of lignocellulosic nanoparticles for emerging applications is presented. My approach is to use simple and green methodology, and to use surface-sensitive characterization techniques to understand interactions and optimize the systems. The significance of the research and its implications on the use of lignocellulosic nanoparticles as a building block for discrete applications, along with its future research prospects are discussed. For a transparent reflection on the work, the limitations of each study and ideas for further research to overcome the drawbacks are also suggested.

5.1 Flame-retardant SBC-CNF aerogels (Publication I)

5.1.1 Effect of sodium bicarbonate on flame-retarding properties

In Publication I, the inclusion of sodium bicarbonate (SBC) on the flame-retarding properties of aerogels intended for insulation applications was evaluated. Sodium bicarbonate has a long tradition of being used as an effective flame-retardant, producing carbon dioxide (CO_2) and water (H_2O) upon heating.[123] However, this was the first report where SBC was incorporated in nanocellulose-based aerogels to enhance their flame-retardancy. Considerable research has been carried out to enhance the flame-retardancy of CNF aerogels but the resulting CNF aerogels either have to surrender their thermal conductivity, or to compromise on the use of unsustainable, toxic, and non-eco-friendly ingredients. To overcome this hurdle, we proposed a greener solution without compromising the CNF aerogel's essential attributes. Subsequently, the data obtained from the horizontal combustion test and thermogravimetry also validated the effectiveness of SBC as a green flame-retardant for CNF based aerogels.

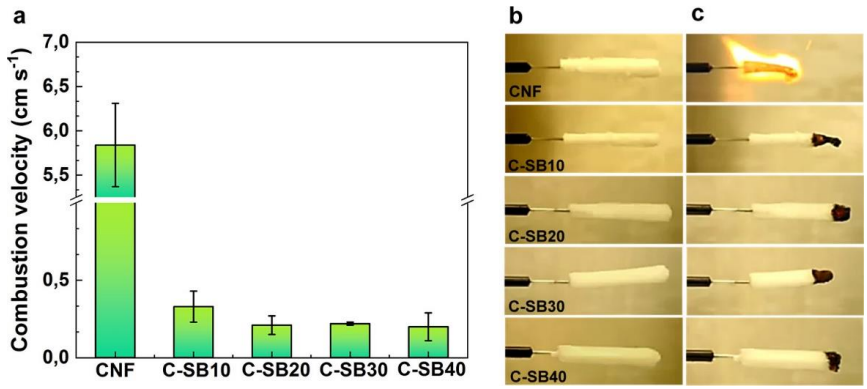

Figure 12. Horizontal flame test of pure CNF and flame-retardant CNF aerogels containing 10–40 wt % sodium bicarbonate. (a) Combustion velocities were determined from the videos recorded during the flame test. Still images of the aerogels (b) before combustion and (c) after 10 s combustion, except for pure CNF where the still image is taken after 2 s of combustion. Reproduced from Publication I.

Pure CNF aerogels readily incinerate in the presence of a flame source but the loading of merely 10 wt % of SBC (C-SB10) imparts a significant effect on the flammability by not only suppressing the flame but also causing a decrease in the combustion velocity (Figure 12). The average combustion velocity exhibited by pure CNF aerogel was 5.84 cm s^{-1}, which by the addition of 10 wt % SBC decreased to 0.33 cm s^{-1}. Further loading of SBC from 10 wt % to 20, 30, and 40 wt % improved the flame retardancy of the aerogels. At 20 wt %, aerogels attained self-extinguishing behavior upon the removal of the flame source. An additional decrease in combustion velocity was also observed for C-SB20, C-SB30, and C-SB40 samples compared to C-SB10, however, the change was minor, as shown in Figure 12.

The information obtained from the thermogravimetric analysis provided further insight into the flame resistance mechanism of SBC and the thermal stability of the aerogels. In the DTG plot (Figure 13 b), the decomposition of pure CNF shows a single distinctive mass loss peak, indicating that CNF decomposed readily in the temperature range of 306–359 °C. In contrast, the thermal decomposition of SBC-containing aerogels exhibited multiple degradation steps. Moreover, the addition of SBC in all the aerogels imparted a noticeable shift in their respective decomposition peaks. Firstly, the peaks shifted toward lower temperature and secondly, the height of the decomposition peaks decreased. The typical SBC peak was nearly absent for C-SB 10 aerogel, indicating molecular scale interaction between the SBC and CNF. At higher concentrations of SBC, its characteristic peak became systematically more prominent. It is evident from the TGA results as well, that SBC undergoes thermal degradation well before CNF, due to which the resulting byproducts Na_2CO_3, CO_2, and H_2O are more likely to interact with CNF. However, the exact mechanism is not known.[123,124]

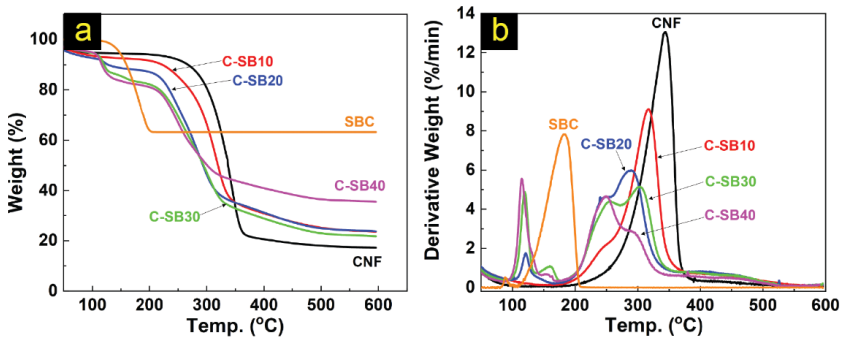

Figure 13. Thermogravimetric analysis (TGA) (a) and derivative thermogravimetry (DTG) (b) curves of sodium bicarbonate, pure CNF aerogel, and flame-retardant CNF aerogels. Reproduced from Publication I.

The emergence of multiple peaks in the flame-retardant aerogels is associated with decomposition processes of different kinetics. As can be observed in Figure 13b, the C-SB 10 aerogel demonstrates a shoulder in the decomposition peak in the temperature zone of 200-270 °C which tends to become more prominent at higher concentrations of SBC. Simultaneously, the decomposition peak maximum which was at 343 °C in the case of pure CNF aerogel moves to 317 °C for C-SB 10 and to 289°C for C-SB20. In the case of C-SB 40, the maximum shifted significantly, reaching 249 °C. This decrease in the decomposition rate brings a positive impact on flame-retardancy. The mechanism behind the fire-retardant feature of SBC is based on energy consumption and the byproducts generated during its decomposition that hinders ignition. During the first stage of burning, decomposition of SBC requires energy to form Na_2CO_2(s), CO_2(g), and H_2O(l). [123] The release of CO_2, on the other hand, limits the oxygen concentration and decelerates the reaction pathway and finally, the released water vapor also consumes further energy. [123]

A successful strategy to improve the flame-retardant property of CNF based aerogels primarily relies on inhibiting ignition, reducing the combustion velocity, and inducing a self-extinguishing attribute, without compromising its porosity, thermal conductivity, and environmental benefits.[125] Self-extinguishing behavior and combustion velocity are important parameters in case of a fire situation. For instance, the rise in temperature makes fire spreading easier. In such a situation, it is efficient to decrease the combustion rate to increase the time available to escape from fires. As observed in our flame test, the incorporation of only 10 wt % SBC, successfully reduced the burning velocity by 94%. Similarly, the self-extinguishing character attained at 20 wt % loading of SBC is also very vital, since it limits the spread of the burning process, resulting in less smoke or gases released during burning.

In recent years, there has been an increasing amount of literature on flame-retardant CNF aerogels. For instance, Wenwen Guo [126], demonstrated the fabrication of flame-retardant cellulosic aerogels by incorporating graphite and red phosphorous with modified morphologies and multiple combinations. Despite flame suppression, the flame-retardant aerogels produced burned out during flameless combustion. The absence of flame or afterglow is still considered a

safety threat since it can spread the fire to other flammables. [125] In the work of Guo et al.,[127] only the CNF–PGN (phosphorus-hybridized graphene nanosheets) aerogel showed competitive flame retardance; however, some caveats such as toxicity related to phosphorus-containing flame retardants and multiple challenges associated with the large-scale industrial production and toxicity of GO needs to be addressed. Yang et al.,[128] and Guo et al.,[113] reported flame-retardancy improvements in CNF aerogels by chemical crosslinking of ultrathin 1T phase molybdenum disulfide (MoS_2) nanosheets and incorporating hydroxyapatite (HAP) respectively. But the shortcoming concerning the use of toxic chemicals and chemical modification of CNF poses challenges for their use. In their attempts, Li et al.,[129] fabricated flame-retardant aerogels by hydrolyzing organosilicon in CNF suspension, and Guo et al.,[112] utilized N-methylol dimethylphosphonopropionamide (MDPA) and 1,2,3,4-butane tetracarboxylic acid (BTCA). Considerable improvement in flame-retardancy was achieved, however at the cost of using corrosive and toxic cross-linking agents, detrimental for both humans and the environment. [130–133]

5.1.2 Effect of sodium bicarbonate on thermal conductivity (λ)

Thermal conductivity (λ) is a vital parameter to evaluate the thermal insulating properties of various materials. The primary use of thermal insulation is to reduce energy consumption, therefore low λ value materials are highly preferred to meet the requirements of thermal insulating materials in buildings and other applications.[134] In this regard, the low densities and high porosities of CNF based aerogels make them efficient thermally insulating materials.[135] However, the addition of a flame-retardant can have a negative influence on the thermal conductivity of the resulting aerogels. In the case of SBC as flame retardant, the obtained λ values demonstrated a promising outcome as illustrated in Figure 14a. The addition of SBC had a very minor effect on the thermal conductivity of the flame-retardant aerogels. Pure CNF aerogel exhibited a λ value of 27.68 mW m^{-1} K^{-1}, whereas at 10% of SBC loading the λ value reached 28.15 mW m^{-1} K^{-1}. The maximum increment was observed for C-SB40 achieving λ value of 28.47 mW m^{-1} K^{-1}, which is merely 0.8 mW m^{-1} K^{-1} higher than the pure CNF λ value.

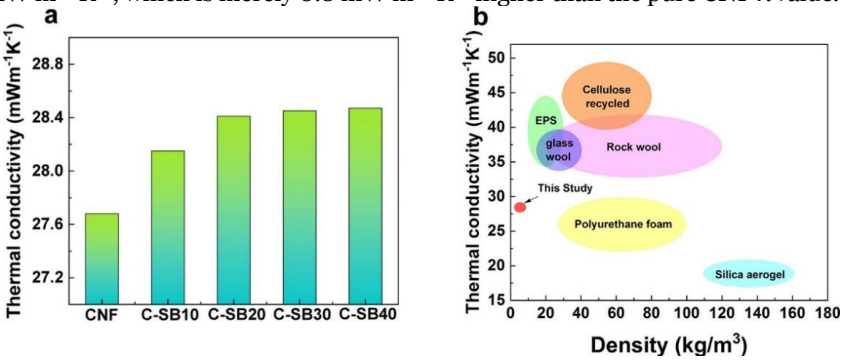

Figure 14. Thermal conductivity values of aerogels. (a) λ values of pure and flame-retardant CNF aerogels. (b) Ashby plot of thermal conductivity versus density for commonly used insulation materials including this study and values obtained from ref[136]. Reproduced from Publication I.

The thermal conductivity values obtained in our work are compared with commercially available insulating materials in Figure 14b. This comparison shows that the flame-retardant aerogels produced by the addition of SBC offer better thermal insulating potential along with very low density. Furthermore, significant flame retardance can be achieved by the addition of SBC to the CNF aerogels without compromising the thermal insulation efficiency, in contrast to many of the earlier studies tabulated in Table 5.

5.1.3 Effect of sodium bicarbonate on aerogel morphology

Another aspect of the flame-retardant aerogels for insulation purposes is their morphology. Factor such as porosity, pore diameter, fibril layer structure, and orientation can have a direct influence on the thermal conductivity of the aerogels. In general, the porosity of the system decreases with increasing solids fraction, which, in return, increases the thermal conductivity of the aerogels. The macroscale porosities of all the produced aerogels in this work were found to be above 99%. On the other hand, the apparent porosity value for pure CNF obtained from the μCT data analysis was 74%, which displayed an increment from 74% to 84% at 10 wt % loading of SBC (Figure 15a). The maximum porosity of 87% was obtained at 30 wt % SBC.

Table 5. Comparison of maximum thermal conductivity and density values obtained for CNF based flame-retardant aerogels from different studies

Maximum λ values obtained	Maximum density values obtained	Ref.
mW m^{-1} K^{-1}	kg m^{-3}	
31	59.4	126
28.09	4.73	128
39.1	87.6	113
46	28.5	129
32.6	10.24	112
28.5	10.5	**Publication I**

Data gathered from multiple sources to compare the effect of different flame-retardants on the respective densities of CNF based aerogels is depicted in Table 5. The competitive analysis provides evidence that the density value obtained in **Publication I** is superior, which is anticipated to render a positive effect on the thermal conductivity value as well.

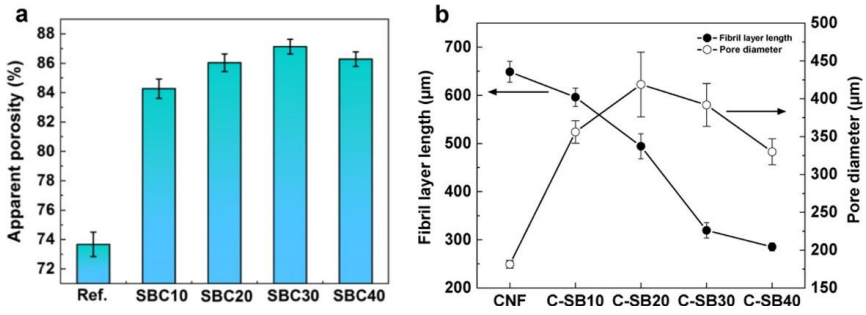

Figure 15. Effect of sodium bicarbonate on the morphology of flame-retardant CNF aerogels. (a) Apparent porosity and (b) mean pore diameter and mean fibril layer length. Reproduced from Publication I.

Moreover, the addition of SBC also resulted in larger pore diameters of 356 µm for C-SB10 and 418 µm for C-SB20, in comparison to the pure CNF, as shown in Figure 15b. At higher loading of SBC, the pore diameter demonstrated a decline to a value of 392 µm for C-SB30 and 329 µm for C-SB40. An increase in the SBC content also caused a loss in the fibril layer connectivity in the aerogel structure. It is expected that the increased heterogeneity of the system, due to the incorporation of SBC, affected the inter and intrafibrillar hydrogen bonding, resulting in loss of fibril connectivity. FESEM micrographs also validated the porosity measurements, showing that the outer surface of the pure CNF has a 2D sheet-like structure with very few pores (Figure 16c). In contrast, the addition of 10% SBC disrupts the sheet structure significantly and continues to shatter the fibril layer structure at higher loading as well. Despite that, the physical integrity of the aerogel was still preserved even at the maximum loading of 40% SBC.

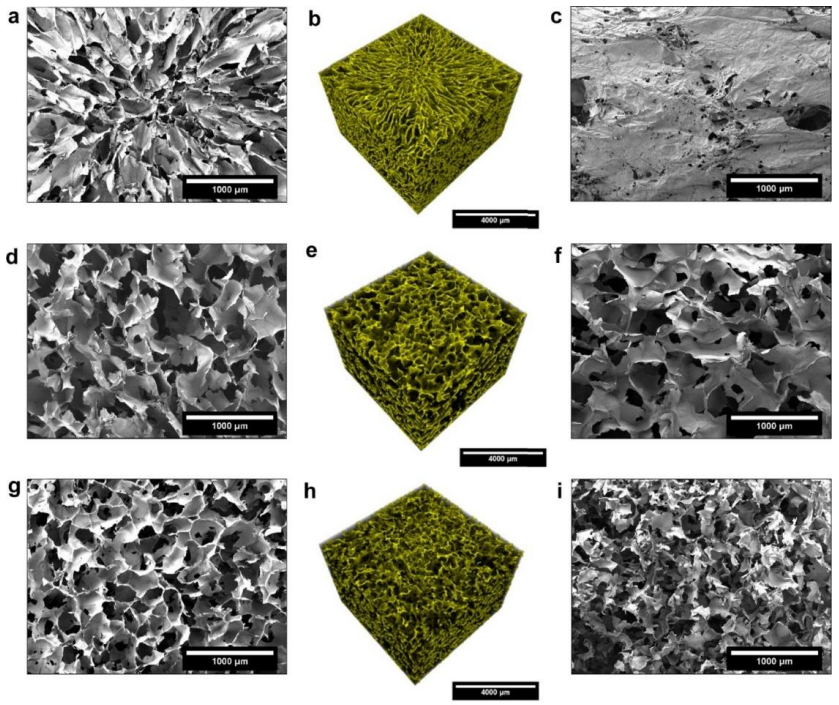

Figure 16. Morphological appearance of pure CNF aerogel and SBC-containing aerogels from FESEM (scale bars 1000 µm) and 3D volumetric rendering (b, e, h) from MicroCT data (scale bars 4000 µm). (a–c) Pure CNF aerogel, (d–f) C-SB10, and (g–i) C-SB30. Reproduced from Publication I.

The use of flame-retardants can have considerable effects on the morphology of the resulting aerogels as observed in Figure 16. Since thermal conductivity is a sum of gaseous, solid, radiative, and convective thermal conductivities, it shows a strong dependence on the density and porosity of the aerogel system.[134] In particular, the inherent high density of certain flame-retardants can result in a loss of the porosity of the aerogel, ultimately increasing the density. Similarly,

the incorporation of a large quantity of a flame-retardant can lead to percolation, providing a path for heat conduction.

5.1.4 Chemical composition

FTIR spectra were obtained to determine the presence of SBC or its possible byproducts in the flame-retardant aerogels. The pure CNF aerogel and flame-retardant aerogels showed similar characteristic peaks in the wavelength region of 2000–4000 cm^{-1}. However, at lower wavenumbers, aerogels combined with SBC presented a new band at 833 cm^{-1}. The presence of this band was associated with the CO_2 bending vibrations present in SBC.[137] A linear relationship between the height of this band and the concentration of SBC was also observed, as shown in Figure 17. Since all the samples have CNF, the peak at 896 cm^{-1}, which is related to β-glycosidic linkages, remains constant for all the samples. Therefore, the ratio of these two bands present at 833 cm^{-1} and 896 cm^{-1} is used as a measure of the increase in band intensity at 833 cm^{-1} which is associated with SBC in Figure 17.

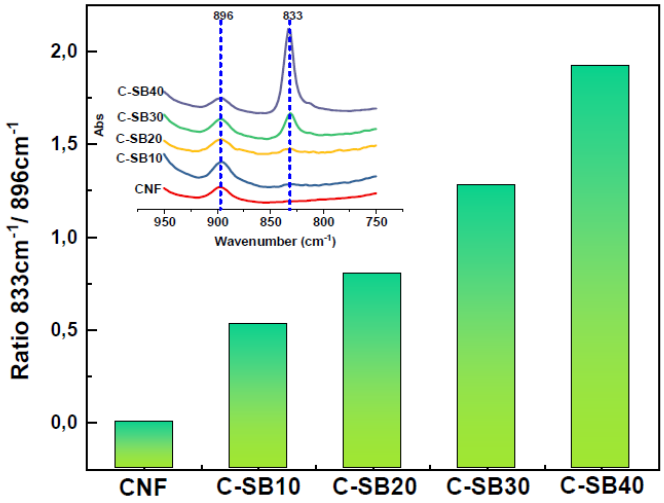

Figure 17. FTIR peak ratio 833cm^{-1}/ 896cm^{-1} as a function of SBC concentration. Reproduced from Publication I.

Taken together, these findings reinforce the use of readily accessible sodium bicarbonate as an environmentally friendly flame-retardant without the need for toxic additives. Most importantly the use of SBC does not induce a negative impact on any of the desirable properties of aerogels for insulation applications. The thermal conductivity values obtained in our work are comparable, or even better, than commercially available insulation materials such as polyurethane foams [20–50 mW m^{-1} K^{-1}], polystyrene foams [30–40 mW m^{-1} K^{-1}], and mineral wool [30–40 mW m^{-1} K^{-1}].[113] Besides having competitive thermal conductivity and lignocellulosic origin, the prepared aerogels generate harmless gases during flameless pyrolysis, making them a promising candidate for a variety of insulation applications.

Like any other study, our SBC containing aerogels also have a few limitations. The current research was not specifically designed to prepare mechanically tough aerogels, therefore, the prepared aerogels were slightly brittle, however mechanically stable to handle without extensive deformation. Another weakness of our reported aerogels is their moisture absorption tendency, which can affect their thermal conductivity in long-term use. The majority of the aerogels presented in literature have been prepared by freeze-drying; however, it is an expensive unit operation and large objects take longer times to freeze-dry. Therefore, the development of a scalable method would be necessary to produce economically feasible CNF based aerogels. The relevance of CNF in sustainable product design is supported by the work above, however, CNF alone has certain limitations. Therefore, it is highly desirable to broaden our understanding of the second component of lignocellulosic biomass, lignin, more specifically in the form of colloidal lignin particles. Improved understanding will enable us to efficiently design products from CNF and CLPs in combination to obtain synergic effects as demonstrated by nature in the plant cell wall.

5.2 Fundamental understanding of CLPs surface properties (Publication II)

In Publication **II**, the second major component of lignocellulosic biomass in the form of colloidal lignin nanoparticles was examined to uncover their peculiar nature and multifaceted surface properties. It was anticipated that to enable optimization of their use in nanocomposite systems, it is important to gain a rudimentary understanding of CLPs, in terms of their interaction with soluble compounds, wetting properties, pH stability, and their spherical geometry. To achieve this goal, well-defined and stable model surfaces from CLPs were prepared. For the preparation of CLPs, two different solvent systems, THF–water, and acetone–water binary mixtures were used, and the resulting CLPs were termed accordingly CLP_{THF} and $CLP_{acetone}$. However, since the nanocomposites discussed in the next chapter were prepared by utilizing only CLPs from the acetone–water binary mixture, most of the following discussion revolves around the surface properties of $CLP_{acetone}$. Due to the homogeneous surface coverage obtained by the adsorption method, model films prepared using this approach were used in the following studies. For comparative analysis, conventional model films from dissolved lignin were also evaluated.

5.2.1 The wetting properties of CLP model surfaces

Model films prepared from both types of CLPs exhibited higher hydrophilic character in comparison to their source lignin material. The water contact angle (WCA) values obtained on films from CLP_{THF}, $CLP_{acetone}$, and dissolved $lignin_{dissolved}$ after conditioning at 15% and 50% RH are shown in Figure 18. The average WCA values for $CLP_{acetone}$ were 32.9 ± 2.3° at 15% RH and 26.8 ± 0.8° at 50% RH, respectively. It is expected that, due to its hydrophilic nature, CLPs adsorb more moisture at higher humidity, which led to a decline in WCA value. On the other hand, the $lignin_{dissolved}$ displayed an average WCA value of 58.5 ± 1.4° at 15% RH and 62.8 ± 2° at 50% RH. Interestingly, the effect of humidity is less pronounced or even opposite for $lignin_{dissolved}$. It is the formation mechanism of lignin nanoparticles, which results in different surface chemistry, that causes the change in WCA values.[77,81] During the nanoparticle self-assembly process, the hydrophobic parts of the lignin molecules organize first due to their low water solubility, inducing a packing orientation of –OH and –COOH functional groups towards the surface, invoking the hydrophilic character in CLPs. [23,138]

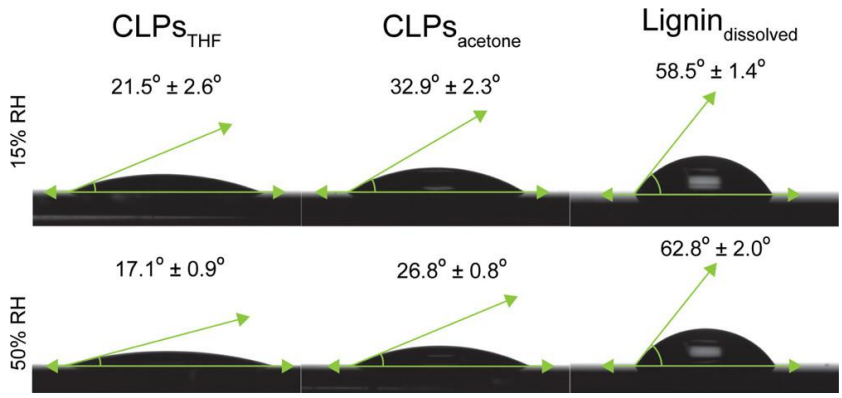

Figure 18. Sessile drop, WCA on CLP_{THF}, and $CLP_{acetone}$ thin films prepared via adsorption and spin-coated $lignin_{dissolved}$ thin films. The films were coated on PLL- and PS-coated silica wafers, respectively. Reproduced from Publication II.

The increased hydrophilicity of CLPs compared to the source lignin is significant, specifically from a nanocomposite fabrication perspective. Since the aim is to utilize CLPs in combination with CNF for nanocomposite applications, it would be necessary to consider the consequences of this surface property on the desired nanocomposite system. First and foremost, one key aspect of lignin-containing CNF nanocomposites is the compatibility of lignin with CNF. The challenge is to homogeneously disperse the lignin into CNF dispersion without aggregating any of the system components. Since the self-assembly process facilitates the CLPs to attain hydrophilic character [118] and at the same time CNF is inherently hydrophilic [47], it is easier to achieve a homogeneous dispersion of both nanoparticles, resulting in better interfacial interactions in nanocomposites. The hydrophilicity of CLPs also makes them viable to disperse in a variety of water-based systems and provide better control over the resulting nanocomposites. Furthermore, the spherical geometry of CLPs is also anticipated to influence their capability to reinforce the nanocomposite by efficiently dispersing and transferring load under stress.

5.2.2 Adsorption of cationic lignin on CLPs

CLPs have many different tunable characteristics; among them, surface functionalization is an integral feature which can determine their interaction with the environment. For certain applications, the surface charge of the CLPs can also be adjusted to tailor their interaction through a simple adsorption process. The adsorption of cationic polymer onto CLPs was studied to regulate the desired properties of a nanocomposite system. For this purpose, cationic lignin (Catlig) obtained from the reaction with glycidyl tetramethyl ammonium chloride (GTMAC) and lignin, having a zeta potential of 17.3 ± 1.9 mV was used as a model adsorbate.

A few studies have investigated the adsorption of Catlig onto the CLPs for the preparation of positively charged lignin nanoparticles.[75,83,118] However, to estimate the resulting surface properties of the c-CLPs, bulk methods such as the

light scattering method or zeta potential measurements are often employed[75,83,118]. The drawbacks of these techniques are their limited ability to detect structural changes and physical state. Therefore, due to the capability of real-time monitoring of the adsorption process and structural changes, QCM-D was utilized to study the adsorption kinetics of Catlig onto the CLPs (Figure 19). The adsorption performed on $CLP_{acetone}$ caused a frequency shift (Δf_3) of 16±0.1 Hz as a function of time, whereas Δf_3 demonstrated by $lignin_{dissolved}$ was mere, 9±1 Hz, as depicted in Figure 19a. The higher adsorbed mass of Catlig onto CLPs in comparison to $lignin_{dissolved}$ indicated that the higher negative charge of the surface of CLPs (−29.5 ± 0.3 mV pH 4.0) dominated the adsorption process, whereas, in the case of $lignin_{dissolved}$, it is probable that the limited availability of the charged carboxylic acid groups on the surface resulted in lower adsorption. Furthermore, the nanoscale spherical nature of CLPs also offers a large surface area promoting the adsorption of Catlig.

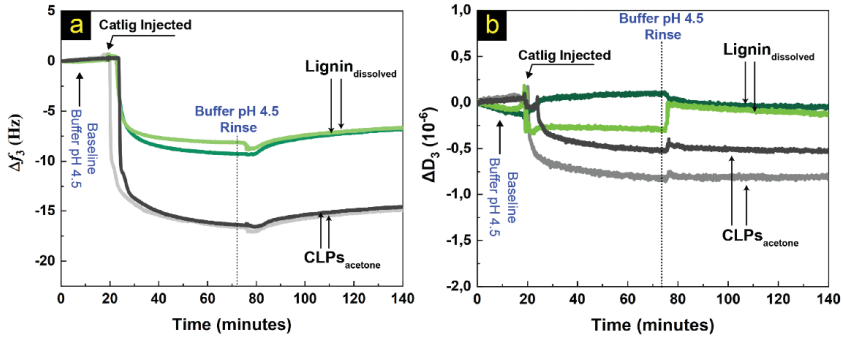

Figure 19. Adsorption of Catlig on CLP films. QCM-D data (third overtone) showing a change in (a) resonant frequency, (b) dissipation response. Reproduced from Publication II.

QCM with dissipation monitoring employed in our measurements also enabled us to quantitatively follow the adsorption behavior and qualitatively analyze the structural properties of adsorbed Catlig layer onto the CLP surface. As we can observe in Figure 19b, the charged groups of Catlig prompted the molecules to adsorb in a flat conformation on the CLP surface, simultaneously causing the release of bound water from CLPs, which can be detected as a decline in the ΔD.

These observations are essential from the viewpoint of surface modification of CLPs by adsorption. Hypothetically, coating the anionic CLPs with a positive charge polymer such as Catlig and then introducing it into the CNF network without precluding the colloidal stability, may improve the adhesion between CNF and CLPs. The addition of crude lignin to a matrix has often resulted in minute improvements in the mechanical properties of the composite systems. In contrast, the large surface-to-volume ratio of CLPs and spherical morphology are also anticipated to provide better dispersion and more efficient interfacial interaction in the nanocomposite components.

5.2.3 pH stability of CLPs

The stability of the CLPs in different aqueous media is relevant to validate their applicability, either alone or in combination, for different application environments. In this regard, $CLP_{acetone}$ thin films were exposed to a pH range from 6 to 12 (Figure 20). After obtaining a stable baseline at pH 6, a stepwise increase in the pH was executed. At pH above 5-6, the degree of deprotonation of the carboxylic and phenolic hydroxyl groups increased, which resulted in the adsorption of water molecules at the CLP surface, which is seen as a decrease in Δf (Figure 20a).

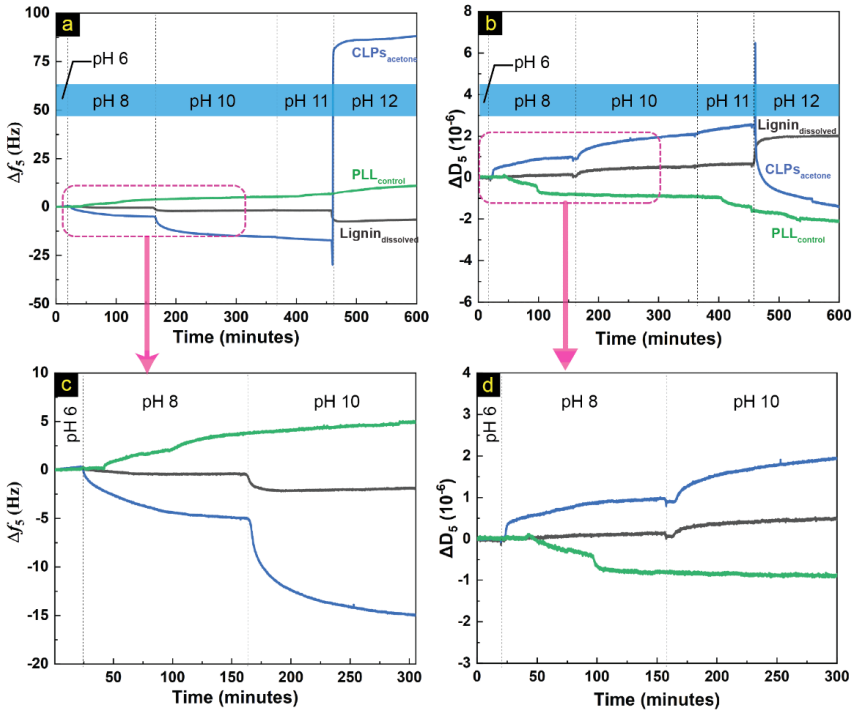

Figure 20. Change in (a) QCM-D frequency and (b) dissipation response, from pH 6 to 12, for $CLP_{acetone}$ and $lignin_{dissolved}$ thin films. (c) frequency and dissipation response (d) for the initial 300 min. Reproduced from Publication II.

At pH 10 to 11, the phenolic hydroxyl groups dissociated, generating an electrostatic repulsion between the lignin chain segments, thus prompting the loss of the outermost layer of CLPs. As a result, the phenolic hydroxyl groups became more accessible. The total dissipation shift (ΔD) for $CLP_{acetone}$ from pH 6 to pH 11 is approximately 2.5 $x10^{-6}$ (Figure 20b), indicating extremely low swelling, low porosity, and a rather rigid nature. After exposure to pH 10, the AFM images revealed a decline in their diameter, resulting from the partial dissolution of low molecular weight lignin fragments. This observation was further validated by the root mean squared (RMS) roughness (Rq) comparison of CLP thin films before and after exposure to pH 10 (Figure 21). CLP thin films remained intact until pH 10 and maintained their spherical morphology, however, a further increase to pH 12 caused complete dissolution of CLPs as shown in Figure 20.

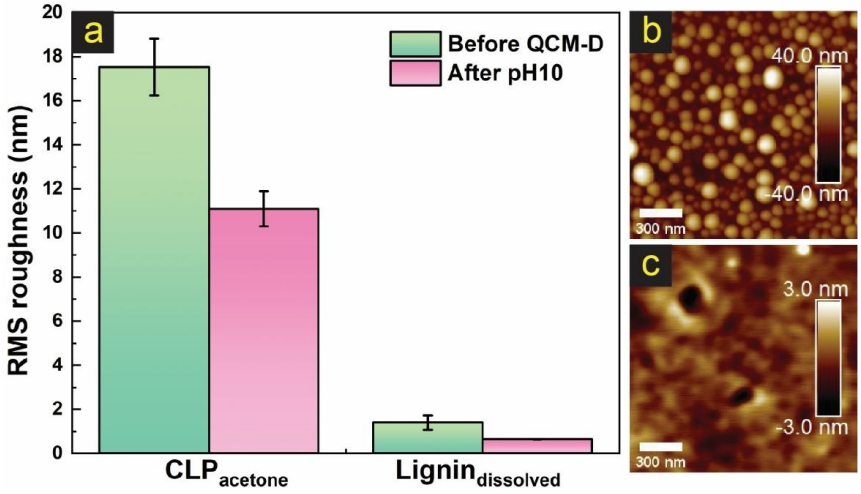

Figure 21. Change in (a) the root mean squared (RMS) roughness (Rq), AFM topographic images, of (b) $CLP_{acetone,}$ and (c) $Lignin_{dissolved}$ thin films after exposure to pH 10. Reproduced from Publication II.

In literature, several studies investigating the stability of CLPs over a wide pH range have relied heavily on zeta potential and particle diameter changes. For instance, Zhi-Hua Liu[139], upon increasing the pH value from pH 7 to 11.0, reported a surface charge of −90 mV along with an increase in the effective diameter of LNPs. The authors associated the high zeta potential value with the excellent stability of CLP in a broad range of pH. Similarly, Tian et al.,[140] reported an increase in particle size at higher pH (>10), which was anticipated to be due to the onset of LNPs dissolution. Another earlier report[73] also employed light scattering and zeta potential measurements to examine CLP stability. In our findings, pH 10 was found to be the cut-off point where the dissolution of the small lignin fragments from the outer surface of CLPs starts to occur as supported by the AFM observations. Furthermore, QCM-D experiments also revealed the rigid nature of the CLPs, providing little room for swelling–deswelling phenomena. It is worth mentioning that the combination of surface-sensitive tools such as AFM and QCM-D played a pivotal role in obtaining detailed information about the state of CLP particles at different pH values. In a recent report, Tao et al.,[141] also utilized the combination of AFM and QCM-D to investigate the pH stability (pH 5 – pH 12) of the crosslinked hybrid lignin nanoparticles. The experimental data obtained revealed valuable information to validate their arguments.

We anticipate that the findings from this study broadens our understanding of CLP surface characteristics and will be relevant for utilizing CLPs for diverse applications. In particular, the use of thin films allowed us to systematically examine the water-binding properties, pH stability, and surface interaction of CLPs on a level of detail not possible with previously used bulk methods. The most obvious finding to emerge from this study is the hydrophilic feature of CLPs, due to the presence of anionic ionizable functional groups at the surfaces.

These functional groups also enabled CLPs to adsorb a higher amount of cationic polymer compared to dissolved lignin. The outcome of these findings indicates that the spherical morphology, tunable surface characteristics, rich hydrophilicity, enhanced availability of surface charged groups, and low degree of swelling, presents CLPs as a potentially versatile option for a multitude of applications as opposed to its source lignin material, hence providing a suitable platform for applications. From a nanocomposite perspective, these findings are highly encouraging and will pave the way to efficiently design nanocomposites from CLPs. In the coming chapters, two different applications of CLPs, a nanocomposite system based on CLPs and CNF, and CLPs as active carriers are designed and discussed in detail.

5.3 Composite films from cellulose nanofibrils and colloidal lignin particles (Publication III)

The improved understanding of CLP surface characteristics and morphological benefits enabled us to efficiently design a nanocomposite system comprised of CLPs in combination with CNF. Different parameters, such as lignin morphology, the concentration of CLPs, surface charge, and drying conditions, were considered to evaluate their effect on the resulting properties of the nanocomposites films. The lignin content was 0, 2, 5, 10, 20, and 50 wt % of the total dry weight in the CNF–lignin suspension. The Z-average particle diameter (nm) and ζ-potential (mV) values are tabulated in Table 6. The photographic presentation of lignin-containing films prepared is given in Figure 22.

Table 6. Particle size distribution and ζ-potentials of colloidal lignin particles and Kraft lignin suspension.

Material	Z-average particle diameter (nm)	PdI	pH	ζ-potential (mV)
CLPs	102 ± 1	0.22	4.3	-25.4 ± 1.3
c-CLPs				
Catlig/CLP 50 mg g^{-1}	708a,b	0.59	3.7	+5.8 ± 0.5
Catlig/CLP 100 mg g^{-1}	147 ± 1	0.18	3.7	+23.0 ± 0.8
Catlig/CLP 150 mg g^{-1}	140 ± 1	0.16	3.7	+23.8 ± 0.5
Catlig/CLP 200 mg g^{-1}	142 ± 1	0.14	3.7	+26.4 ± 0.3
Catlig/CLP 300 mg g^{-1}	132 ± 1	0.14	3.7	+25.1 ± 1.0
Kraft lignin suspension	832 ± 57a		4.9	-22.3 ± 0.6
Catlig	n.a.	n.a.	4.0	+22.1 ± 0.4

PdI, polydispersity index from light scattering. n.a., not analyzed. a: Unstable dispersion b: single measurement.

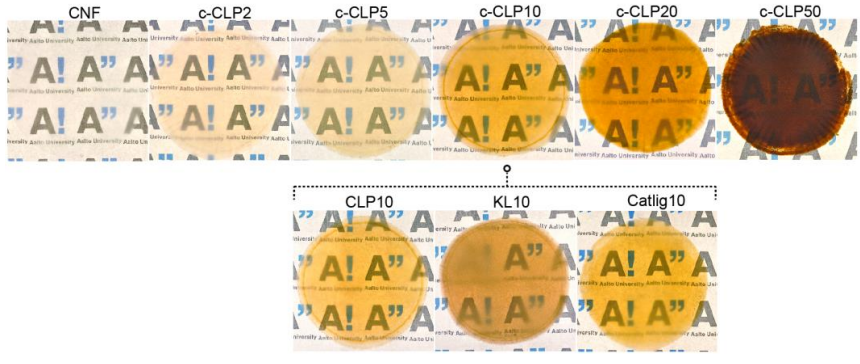

Figure 22. Digital photographs of the CNF and CNF-lignin nanocomposite films. The logo is used with permission from Aalto University.

5.3.1 Mechanical properties of CLP containing nanocomposites

To benefit from electrostatic interactions, CLPs with cationic charge (c-CLPs) (Table 5), were introduced into CNF suspension at different concentrations and charges. A comparative investigation of the tensile properties of lignin–CNF nanocomposites revealed differences between films that contained different lignin types, concentrations, surface charge, and drying conditions.

Effect of c-CLP concentration

The addition of 2 wt % c-CLPs into the CNF network enhanced the mechanical properties of the ambient dried nanocomposite films compared to pure CNF as depicted in Figure 23. The pure CNF film exhibited a tensile strength of 132.0 MPa and strain at a break of 9.4%, whereas, 2 wt % loading of c-CLP increased the tensile strength to 145.7 MPa and strain-at-break to 12.2%. Tensile results obtained at 10 wt % inclusion of c-CLPs revealed a significant increase in mechanical properties with a tensile strength value of 160 MPa and strain-at-break of 16.2%. The large increase in the strain-at-break along with tensile strength resulted in twice the toughness value (15.9 MJ m^{-3}) compared to that of the pure CNF film (8.2 MJ m^{-3}). The further increase in the c-CLP content in nanocomposite films resulted in a decline in both tensile strength and strain values. CNF films with 20 wt % c-CLPs content exhibited a tensile strength of 61 MPa and strain-at-break of 7.5%, whereas additional deterioration in the mechanical properties was observed for 50 wt % c-CLPs.

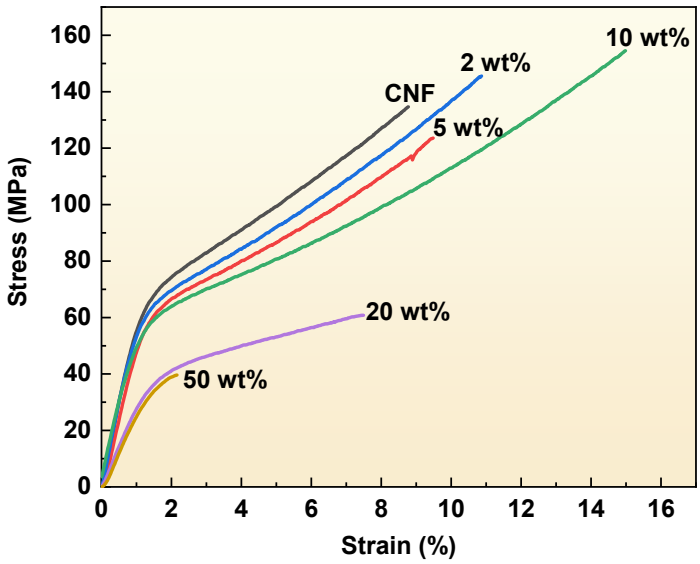

Figure 23. Stress-strain curves of nanocomposite films at different concentrations of c-CLPs.

Effect of c-CLP charge

Due to the optimum tensile properties demonstrated by CNF films at 10 wt % loading of c-CLP, this composition was selected to investigate the effect of the c-CLPs charge on the mechanical properties of the resulting nanocomposite films. To tailor the charge on c-CLP surfaces, the ratio of cationic lignin to CLP was altered from 50 to 300 mg g^{-1}. The tensile data presented in Figure 24 reflect only a minute difference in the mechanical properties of the prepared films. Also, except for the lowest Catlig/CLP ratio of 50 mg g^{-1}, the ζ-potential values of the prepared c-CLPs were within the same range. The charge on the CNF surface is also very low, therefore it was anticipated that electrostatic interactions did not significantly influence the mechanical properties of the nanocomposite films.

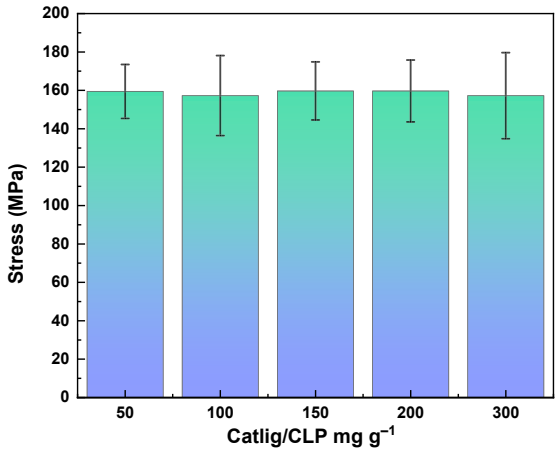

Figure 24. Effect of Catlig/CLP charge ratio on tensile stress of nanocomposite films.

Effect of lignin morphology

To investigate the morphological influence of different lignin types on the mechanical properties, nanocomposite films at 10 wt % loading of regular CLPs, c-CLPs, Catlig, and Kraft lignin (KL) were prepared. Interestingly, the film prepared from CLPs displayed comparable strength and strain at break value as exhibited by positively charge c-CLPs (Figure 25). In contrast, Catlig incorporation resulted in lower toughness values.[142] Compared to c-CLPs and CLPs, the KL nanocomposite film, containing weakly anionic and irregular large lignin particles prone to aggregation, showed lower strength and toughness.

The strain-at-break values of all films were not largely affected by the lignin morphology, as can be observed from Figure 25. The strain-at-break of CLPs, c-CLPs and Catlig were within the same range, but unexpectedly the 10 wt % KL films demonstrated an unprecedented strain-at-break value of 17.8% (±2.1%), exceeding all the values obtained in this work. However, in the case of toughness, it was spherical lignin nanoparticles that provided the best results, regardless of surface charge.

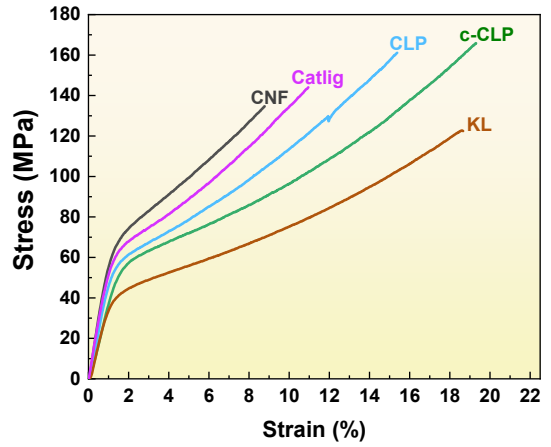

Figure 25. Stress-strain curves for pure CNF and nanocomposites films at 10 wt % loadings of CLPs, c-CLPs, and KL.

Effect of drying conditions

Drying conditions are foreseen to influence the mechanical properties of the cellulosic materials significantly.[121,143,144] Similar trends were also observed for nanocomposite films during our findings. To analyze the effect of hot-pressing and ambient drying, two nanocomposites films at 10 wt % loading of CLPs and KL were prepared. Pure CNF films were also prepared at both drying conditions.

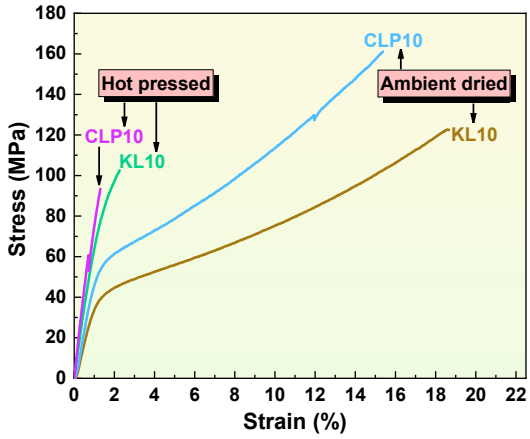

Figure 26. Effect of drying conditions on nanocomposite films prepared at 10 wt % loadings of CLPs and KL, respectively.

As expected, the hot-pressed films demonstrated significantly lower strain-at-break values as compared to their counterparts dried at ambient conditions (Figure 26). This decrease in ductility was also accompanied by a loss in strength. It is deduced that hot pressing led to the compaction of fibrillar layer structure and loss in the porosity of the network.[47,145] CNF based films readily adsorb moisture due to their hydrophilic nature;[146] as the water molecules penetrate between the fibrils they act as lubricating agents.[147] Upon removing water by hot-pressing, additional bonds between the fibrils are constructed, leading to a restricted movement of fibrils[145,148]. All nanocomposite films prepared through the heat treatment drying method exhibited an increase in their respective Young's modulus. It is expected that heat treatment under load causes the densification of the nanofibril network structure, which in turn increases the physical bond between the fibrils,[47] limiting the fibril sliding; therefore films possess low strain-at-break values and high modulus.

It is surmised that, at the optimum content of CLPs and c-CLPs, the synergetic effects of multiple factors lead to an increase in the mechanical properties. Under load, cellulose nanofibrils slide, causing a cascade of hydrogen bond breaking and reforming along with fiber fracture, which consequently leads to network failure. [149,150] Since the CLP surface is also rich in hydroxyl functional groups it is anticipated that they will act as lubricating agents and will enhance the cascade events of hydrogen bonding breaking and reforming under load. The possible mechanism behind the improved toughness of CLP and c-CLPs

nanocomposite films is deduced from the FESEM micrographs of the nanocomposite films as depicted in Figure 27.

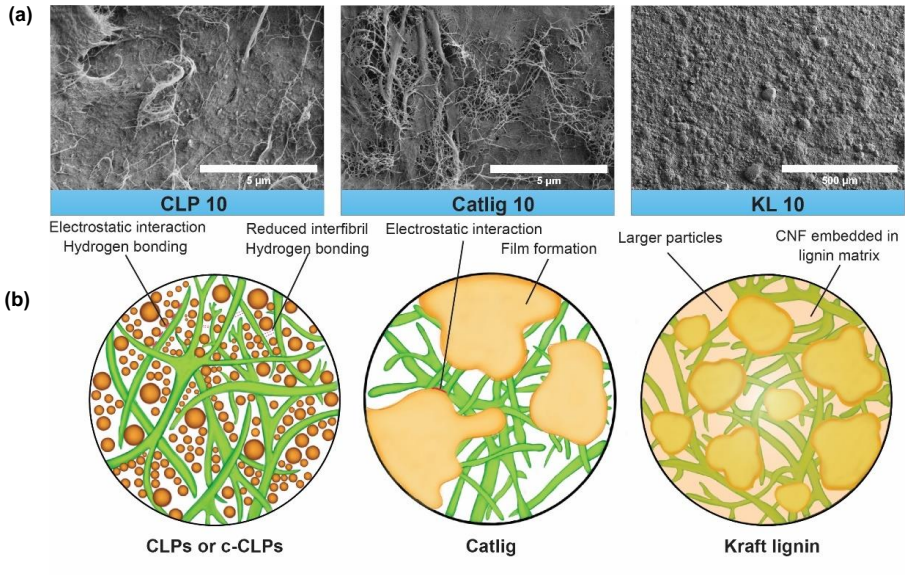

Figure 27. FESEM micrographs (a) of CLPs, Catlig and KL nanocomposite films at 10 wt % loading, (b) Schematic illustration of the proposed interaction between CNF and different lignin morphologies. Note: Image is not drawn to scale.

The well-defined spherical geometry of CLPs and their hydrophilic character allow them to disperse well into the CNF network. Their presence in the CNF network might reduce the intrafibrillar hydrogen bonding; however, the abundance of hydroxyl on their surfaces leads to the formation of strong particle-fibrillar hydrogen bonding. Furthermore, the hydrophilic nature of both the nanoparticle CNF and CLP enabled them to retain water molecules on their respective surfaces. Upon the application of stress, CLPs act like ball-bearing lubricating agents, transferring the stress, and consequently improving the ductility and toughness in the nanocomposite. The presence of a thin layer of water molecules at the CNF-CLPs contact zone further promotes the smooth sliding movement.[147] In contrast, the higher content of c-CLPs (50 wt %) drastically reduced the intrafibrillar interactions due to the disruption of the fibril layer structure, which resulted in poor mechanical properties. It was expected that the electrostatic interactions would play a decisive role in the mechanical properties of nanocomposites films. Nevertheless, the results obtained from negatively charged CLPs and positively charged c-CLPs nanocomposite films demonstrated similar mechanical properties. These observations led to the conclusion that the role of hydrogen bonding is more dominant in CNF nanocomposites compared to electrostatic interactions.

Before this work, CNF films containing residual lignin had been studied extensively.[151–154] However, no study existed which would have adequately covered the effect of CLPs with spherical geometry on the mechanical properties of the nanocomposite films. On the other hand, most studies aimed to utilize CLPs for biobased nanocomposites have mainly focused on biopolymeric systems such

as PVA,[93,97,98] and PLA, [100] with rare reports on CNC [100] and chitosan [96]. The comparative analysis of the property enhancement in biopolymer-based CLP nanocomposite systems reveals minor improvements, especially in mechanical properties. Yang et al.,[100] prepared CLP/PLA nanocomposites by solution casting the mixture of CLPs (0, 1, and 3 wt % of CLPs) and PLA, which demonstrated decreased tensile properties. The CLPs utilized in their work had a mean diameter of 40 to 60 nm, however, the FESEM images reveal a non-spherical cluster of irregular particles (200-250 nm). It is known that to attain a homogenous dispersion of CLPs into polymeric systems, the shape and individual well-defined particles are of vital importance.[155] Therefore, the detrimental effects of CLPs on the nanocomposites observed in the reported work of Yang et al.,[100] can be attributed to inhomogeneous dispersion of lignin nanoparticles into the PLA matrix. In a similar work, Yang et al.,[156] also prepared CLP/PLA nanocomposites and reported an increase in tensile properties. However, the improvement in tensile strength was only approximately 10 MPa. Furthermore, the micrograph of CLPs shows a large cluster of layered morphology and non-spherical nature. In an attempt to prepare PLA/CLP nanocomposites, the Pickering emulsion method was utilized by Li et al.[157] The tensile strength and strain decreased with the increased amount of CLPs. The reported particle size of CLPs was 55 ± 9 nm, but FE-SEM images suggest the lignin particles are not stable but form larger clusters. Yang et al.,[99] study aimed to increase the strength of wheat gluten by incorporating 0, 1, and 3 wt % of CLPs, also revealed only a small increment in tensile strength of just 8 MPa.

5.3.2 Water interactions of lignin-nanocomposite films

Water plays a significant role in all biomaterials, and the nature of water and its mobility has attracted renewed interest in various engineering and science fields.[158] Therefore, the interaction of water with lignin-containing nanocomposite films was of immense interest to us. Data obtained from DVS, thermoporometry, and water permeability tests offered fascinating insights, as discussed below. Apart from influencing the mechanical properties of nanocomposite films, the presence of CLPs also affected their interaction with water.

The water permeation tests revealed that the nanocomposite films prepared at 2, 10, and 20 wt % loadings of c-CLPs, dried at ambient conditions, acquired water resistance character (Figure 28), in contrast to the pure CNF films that were permeable to water. Similarly, nanocomposite film prepared at 10% loading of CLPs also demonstrated water resistant behavior. The hot-pressed CNF films also attained a water resistance feature.

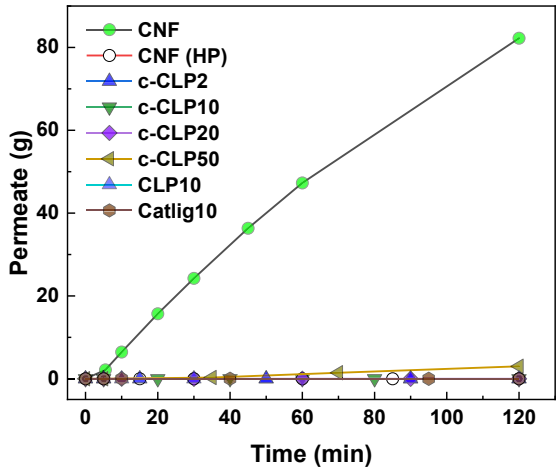

Figure 28. Effect of hot pressing and lignin content of different morphologies on water permeation of the CNF and CNF-lignin nanocomposite films. Reproduced from Publication III.

The reason behind this change in water permeation behavior is understood by analyzing the data provided by thermophotometry. It was noticed that the films containing CLPs exhibited a higher percentage of pores in the mesoporous region. For an instant, ambient dried CNF and CLP10 nanocomposite film possess overall similar porosity, but the CLP10 nanocomposite film retained a higher percentage of pores in the mesoporous range (Figure 29a). It is surmised that the hydrophilic nature of CLPs plays a critical role in the porosity of the nanocomposite. During the drying stage, the higher surface tension of water causes capillary condensation as the water molecules evaporated, which led to the formation of a high number of pores in the mesoporous region. The presence of a large number of small pores exerted high capillary pressure, restricting the permeation of water through the film.

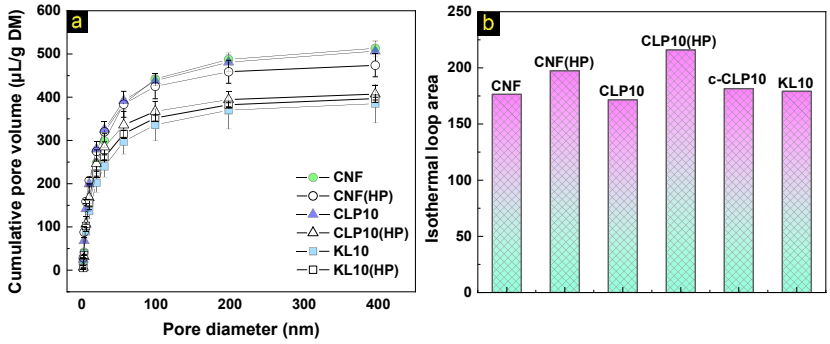

Figure 29. (a) Comparison of the mathematical loop area of the sorption isotherm. (b) cumulative pore size distribution based on tp-DSC for CNF and lignin–CNF nanocomposite films. Reproduced from Publication III.

Water interaction in terms of moisture sorption tendencies of pure CNF and nanocomposite films at 10 wt % lignin content are depicted in Figure 29b. Ambient dried CNF, CLPs, and c-CLPs films showed similar magnitudes in the isotherm loop area, indicating that the total amount of hysteresis demonstrated by

all the tested ambient dried films is similar. The sorption isotherm reveals that until 50% RH, both pure CNF and nanocomposite films exhibit minor differences in their respective sorption isotherms. However, at higher RH, they display different equilibrium moisture content (EMC) values. In brief, at the highest RH of 95%, the ambient dried films present larger EMC values as compared to the hot-pressed ones. The lower EMC values of hot-pressed films are most likely the result of the loss of cumulative pore (Figure 29b) volume and densification of the fibrillar network.

The results of this research support the idea of harnessing the collective potential of lignocellulosic nanoparticles for composite applications. The unique nanoscale structural features of both nanocellulose and colloidal lignin nanoparticles such as high aspect ratio, large specific surface area, and presence of functional groups on their respective surfaces make them an ideal combination in which both matrix and reinforcement are of biological origin.

The present approach has several attractive features; both nano-components CLPs and CNF demonstrate excellent suitability for water-based systems and contribute to property enhancements without the need for any chemical modification to either CLPs or CNF.[142] Finally, the important limitation needed to be considered is the hydrophilic nature of both CLPs and CNF. The hydrophilic surface character not only limits their applications but also prevents the use of hydrophobic polymers, making them incompatible for nanocomposite applications. To overcome this concern, the next study utilizes the water-based PU system in combination with CNF to selectively hydrophobize one side of the composite film.

5.4 Cellulose nanofibril composite films with polyurethane (Publication IV)

5.4.1 Water interaction of CNF-PU films

During nanocomposite film preparation, PU particles concentrated towards the bottom side of the films due to the vacuum gradient. The nanocomposite films obtained exhibited a top surface rich in CNF and a bottom surface enriched with PU. This arrangement of two distinctive materials in one film rendered the films stereoselective and significantly influenced their water interaction properties. The nanocomposite film at 10% PU fraction exhibited a WCA value of 81° towards the PU-rich surface, and 30° towards the CNF-rich surface as shown in Figure 30. Similar trends in WCA values were observed at different loading of PU content, as tabulated in Table 7.

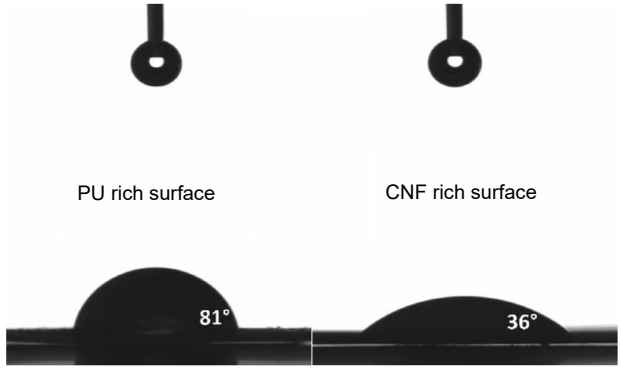

Figure 30. Water contact angle images of CNF/PU nanocomposite at 10 wt % PU content. Reproduced from Publication IV.

Table 7. Water contact angle values for pure and CNF-PU nanocomposites

Pure PU		81.3° ± 1.3°
CNF(10)PU	PU rich surface	81.4° ± 1.2°
	CNF rich surface	36.1° ± 1.3°
CNF(30)PU	PU rich surface	62.5° ± 3.2°
	CNF rich surface	37.1° ± 2.2°
CNF(60)PU	PU rich surface	77.9° ± 0.3°
	CNF rich surface	69.8° ± 2.7°
Pure CNF		45.6° ± 8.5°

FESEM micrographs and X-ray photoelectron spectroscopic data also complemented the wetting experiments. FESEM micrograph of the nanocomposite films with 10 % PU, clearly indicated the presence of fibrils on CNF rich surfaces. In contrast, the PU-rich surface depicted a smooth surface, with no signs of fibrils. Likewise, the spectra obtained from X-ray photoelectron spectroscopy also revealed a large number of N-C=O bonds present on the PU-containing surface and a high concentration of the typical carbon bound to only one oxygen (C-O), characteristic for cellulose, on the opposite side of the film.

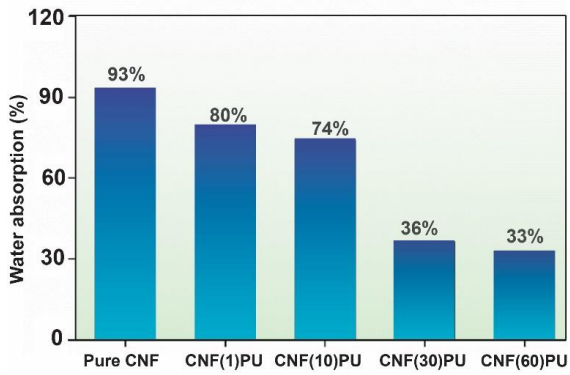

Figure 31. Water absorption of the pure CNF and nanocomposite films. Reproduced from Publication IV.

As shown in Figure 31, the nanocomposite films containing PU demonstrated lower water absorption as compared to the pure CNF films. It is important to mention that it is the PU-rich side which affects the overall absorption of the nanocomposite film. This observation is in line with the previous findings,[142] since the PU brought the hydrophobic character into the films so that the nanocomposite films showed a reduced affinity to water, leading to a decline in moisture absorption.

5.4.2 Mechanical properties of PU containing nanocomposites

Due to the high elongation at break of PU, its introduction into CNF caused a systematic decline in Young's modulus of the PU-CNF composite films, as can be observed from the respective stress-strain plots in Figure 32a. At the loadings of 1, 10, 30, and 60 wt % of PU, the reduction in the modulus was 9%, 20%, 50%, and 70%, respectively, as compared to the pure CNF films. In the same fashion, the tensile strength of the nanocomposite films also exhibited a decline upon the incorporation of PU. However, in contrast, and more importantly, the CNF-PU nanocomposites demonstrated excellent wet strength properties, when wetted from the PU rich side, depicted in Figure 32b. The PU-CNF nanocomposite at 10% of PU loading showed a modulus of 3.9 GPa, which was 400% higher than the pure CNF film. Similarly, at the loadings of 1, 30, and 60 wt % of PU, the improvement in Young's modulus was 150%, 300%, and 100% higher than for the pure CNF film, respectively. Apart from tensile modulus, the CNF-PU nanocomposites also revealed significantly higher tensile strength as compared to the pure CNF film. The deformation behavior of the PU-CNF nanocomposites showed a characteristic stress-strain curve as obtained for dry samples; however pure CNF film under wet conditions failed to exhibit the yielding region, rather it started deforming inelastically. Wetting of the CNF rich side of the nanocomposites for tensile testing failed to show any significant improvement.

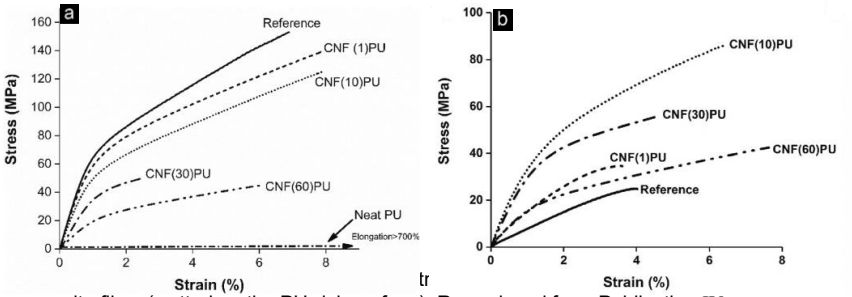

tr -
composite films (wetted on the PU-rich surface). Reproduced from Publication IV.

A clear benefit in the wet strength of CNF nanopaper can be observed from the strategy employed in the presented work. Since it's the wet resistance of the CNF films which hinders their commercialization, a considerable amount of literature has been published on surface modification of the CNF surfaces to achieve competitive water resistance. Chemical methods are often employed to hydrophobize the CNF surfaces, among which esterification is commonly practiced.[159–162] Similarly, the introduction of substituted silyl groups onto the surface of CNF and carbamination by reacting isocyanates and the hydroxyl groups of the cellulose have also been practiced to obtain hydrophobic CNF materials.[163] The major drawback of chemical modification of CNF before film formation is the loss in mechanical properties of the CNF films due to their detrimental effects on the hydrogen bonding between the fibrils. A combination of CNF with water-based polymers has also been utilized in this regard. Henriksson et al.,[164] mixed water-based melamine formaldehyde in CNF dispersion to prepare nanopapers which demonstrated higher modulus and improved yield. Another approach to gain wet strength was employed by Lucenius et al.,[165] where the inclusion of uncharged polysaccharides improved the wet strength of CNF films.[47,166]

In a nutshell, the results obtained from PU containing CNF nanocomposites confirm the previous finding of the suitability of CNF for water-based systems to obtain nanocomposites with excellent properties. The raw materials utilized, CNF and PU, are both readily available in large quantities, making them ideal for large-scale industrial applications. The hybrid wetting properties are unique assets of these nanocomposites, which makes them well suited for applications where the CNF-rich surface, due to its barrier properties, and PU-rich surface, due to its hydrophobic character, are required. Still, the use of PU may raise concern since it is not biodegradable. However, it is anticipated that, by using a relatively small amount (10 wt %) of PU, considerable improvement in water resistance can be gained. Furthermore, the comparative methods used to obtain hydrophobicity also have certain consequences. First and foremost, after targeting the hydroxyl groups for surface modification, the hydrogen bonding of the CNF films has to be sacrificed, making the films mechanically weak; it often also deteriorates their barrier properties.[167–169] Furthermore, the unhealthy, toxic, or dangerous chemicals and solvents used in certain surface modifications are cer-

tainly not encouraging concerning the environment. Last but not the least, direct chemical modification makes the nanocellulose less biodegradable or non-biodegradable.[92]

5.5 CLPs as activating anchors for enzymatic ester synthesis in aqueous conditions (Publication V)

This work aims to utilize the prominent surface features of CLPs. We exploited the significant negative charge of the CLPs to adsorb lignin that had been modified to carry a positive charge to produce cationic CLPs. The adsorption of Catlig onto the CLPs was verified in Publication II. The cationic CLPs were used as enzyme carriers for ester synthesis.

5.5.1 Enzymatic synthesis of butyl butyrate in aqueous-organic media

The esterification of butyl butyrate is of considerable industrial interest due to many applications as additives for food products as flavoring compounds and in cosmetics. However, the presence of water has retardation effects on esterification kinetics due to reverse hydrolysis. An innovative method to proceed with ester synthesis in water by fabricating enzyme immobilized cationic lignin nanoparticles entrapped in calcium- alginate was designed. To estimate the aqueous esterification of this new system, the synthesis of butyl butyrate commenced. After 24h reaction time, Lipase M adsorbed on the surface of c-CLPs, entrapped inside alginate beads, which exhibited a maximum molar yield of 34% in the biphasic hexane- water (1:1, v/v) medium (Figure 33). After five consecutive reaction steps, the molar yield of butyl butyrate was competitive to the yield obtained in the first 24 h reaction from the alginate beads containing only Lipase M. Furthermore, the Lipase M enzyme adsorbed on c-CLP entrapped in alginate showed a molar yield of 70% as compared to only 2% from LbL-coated catalysts after 96 h. Experimental evidence suggested that entrapment of Lipase M with Catlig had a beneficial outcome on the esterification performance, associated with the activation and anchoring effect.

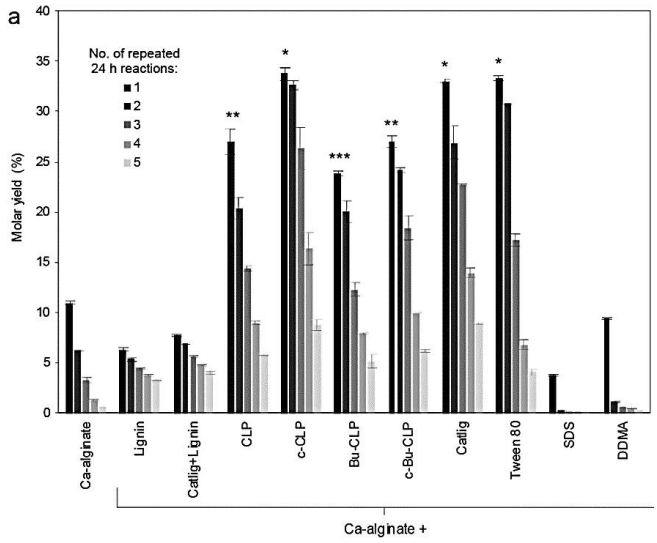

Figure 33. Biphasic butyl butyrate synthesis catalyzed by Ca-alginate beads containing Lipase M, various forms of lignin, or surfactants. Comparison of various surface-active materials in Ca-alginate beads used in five repeated 24 h reactions.

The esterification reaction catalyzed by the Lipase M adsorbed on c-CLP and entrapped in the Ca-alginate matrix proceeds in two stages. In the first stage, the reagents butanol and butyric acid diffuse into the alginate beads containing the enzyme from the aqueous-organic medium and reaches the confined enzyme space. In the second stage, the low solubility of the butyl butyrate[170] causes its diffusion from the confined enzyme space into the Ca-alginate matrix and ultimately into the external organic phase. The Ca-alginate serves as a water-absorbing matrix and resists swelling which maintains a low water activity in the vicinity of the enzyme. Due to the presence of organic solvent in the reaction medium, the synthesized product is continuously removed, which drives the reaction toward products.

5.5.2 Activation of lipases by synthetic surfactants

To evaluate the efficiency of our immobilization strategy compared to the use of surfactants, Lipase M was entrapped in alginate hydrogel with nonionic, anionic, and cationic surfactants, Tween 80, sodium dodecyl sulfate (SDS), and didodecyl dimethylammonium bromide (DDMA), respectively. The nonionic surfactant, Tween 80 demonstrated the highest butyl butyrate yield, equivalent to the one obtained by Catlig after two 24 h reactions (Figure 33). On the other hand, SDS and DDMA surfactants exhibited negligible yield due to their structural configuration. It is anticipated that the presence of aromatic species and the complex three-dimensional structure of Catlig anchors the Lipase M effectively, leading to better yield. Moreover, during the immobilization step, Lipase M adsorbed onto c-CLPs formed spheroidal clusters before being entrapped into the alginate hydrogel, illustrated in Figure 34a.

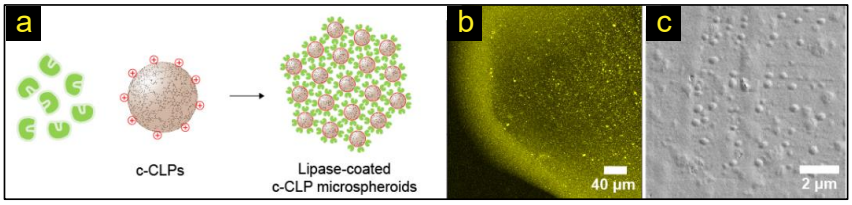

Figure 34. (a) Schematic illustration of the interfacial activation and confinement of hydrolases entrapped after adsorption on c-CLPs. (b) confocal laser scanning microscopy (CLSM) and (c) FESEM images display corresponding microstructure assembly in the calcium alginate matrix.

Many studies have demonstrated the use of different lipases for a variety of reaction systems, however, the molar yield obtained in this work for butyl butyrate is among the highest reported for biphasic,[171] microaqueous,[170], or non-aqueous[172] reactions. Gomes et al.,[173] utilized Chitin-immobilized lipase for synthesizing butyl butyrate[173], which delivered a molar conversion yield of 69% in 48 h. Synthesis of methyl butyrate in 9:1 v/v hexane: water returned a molar yield of 40% in one hour; however, the synthesis was accomplished using free lipase, and catalyst recycling was neglected.[174] Another report demonstrating the immobilization of Lipase in alginate beads containing hexadecane only managed

to obtain a 32% molar yield of butyl butyrate in 96 h, after excessive extraction.[171]

Taken together, the present work demonstrates the effective utilization of the surface features of CLPs for ester synthesis in aqueous media. An efficient design of these microreactors was only possible due to the anionic nature of CLPs and their large surface area. Furthermore, the system provided multiple advantages over existing techniques. Spatially confined lipase retained 70% of its synthetic activity at higher water to hexane volume ratio (9:1) in the reaction medium. Importantly, lipase immobilization does not require cross-linking, eliminating the need for cross-linking agents [173,175] along with excellent stabilization of the enzyme under esterification conditions.

6. Conclusions

By effectively utilizing the nano-components of lignocellulosic biomass, this thesis has demonstrated that the nano-morphologies of cellulose and lignin in the form of cellulose nanofibers and colloidal lignin particles respectively, are likely to play a pivotal role in providing greener solutions, from high-tech and novel products to bulk consumables. The strenuous challenges posed by the flammability and hydrophilicity of nanocellulose and secondly, structural diversity and heterogeneity of lignin, were addressed using novel approaches. This work also highlights the importance of surface-sensitive methods such as QCM-D and AFM to obtain the greater understanding necessary for designing lignocellulosic materials in optimum fashion.

From the application perspective, a significant improvement in the flame retardancy of CNF aerogels without compromising their insulation properties and thermal stability was made possible. The use of SBC provided excellent flame-retardancy to meet the strict safety requirements for building insulation, along with paving the way for a low-cost, industrially efficient, and environmentally friendly method. To expand our focus towards the development of nanocomposite systems for harnessing the collective potential of both CNF and CLPs, a systematic examination of CLPs was performed. The analytical platforms, QCM-D and AFM provided a detailed understanding of CLP, in terms of their surface interactions, wetting properties, and pH stability, on a level of detail not possible with previously used bulk methods. An efficient design of the nanocomposites from CNF-CLPs demonstrated tougher film structure along with the highest strain at failure values reported thus far for all-lignocellulose films. We anticipate that the unique nanoscale structural features of both CNF and CLPs such as high aspect ratio, large specific surface area, and spherical geometry of CLPs, in combination with rich functional group surface, contributed synergistically to enhance the toughness of nanocomposites. Learning from the encouraging results from CNF-CLP nanocomposites, the challenge of the inherent hydrophilicity of CNF was addressed by preparing CNF-PU hybrid nanocomposites. The hybrid nanocomposites acquired stereoselective water-resistance character, being hydrophobic towards the PU-rich side and hydrophilic on the CNF-rich side. The addition of low PU content remarkably enhanced the wet strength and decreased the water absorption of the material. Moreover, the an-

ionic nature of CLPs and their large surface area was utilized to prepare microreactors by immobilizing enzymes for ester synthesis in aqueous media. The enzyme immobilizing CLPs embedded in alginate beads demonstrated remarkably high synthetic activity retention in the presence of a large quantity of water, providing an environmentally friendly and affordable solution to control the reversibility of hydrolases.

While this thesis answered many questions, at the same time some limitations were also observed. For instance, the flame-retardant CNF aerogels were slightly brittle. Another weakness regarding these aerogels is the increase in moisture absorption at a high loading of sodium bicarbonate, which may affect their thermal conductivity in long-term use. The affinity of CNF and CLPs to water, resulting from their chemical structures, offers many advantages such as their utilization in water-based systems, but it also brings along the limitation of their use with hydrophobic polymers because of poor dispersion or compatibility. This challenge can be addressed by using a polymeric system such as water-based polyurethane, but it is not biodegradable, even though PU was used in very low quantity.

Central to the entire thesis work was the use of lignocellulosic building blocks as a material platform for diverse applications. In light of the opportunities and limitations posed by CNF and CLPs, further development of their surface character would be necessary to expand their application portfolio. However, any such surface modifications to CNF or CLP, which can compromise their biodegradability must be avoided. Furthermore, the use of toxic and harmful reagents should be minimized as much as possible to preserve the environmentally friendly nature of lignocellulosic materials.

7. References

(1) D'Amato, D.; Veijonaho, S.; Toppinen, A. Towards Sustainability? Forest-Based Circular Bioeconomy Business Models in Finnish SMEs. *For. Policy Econ.* **2020**, *110* (October 2018), 101848. https://doi.org/10.1016/j.forpol.2018.12.004.

(2) De Besi, M.; McCormick, K. Towards a Bioeconomy in Europe: National, Regional and Industrial Strategies. *Sustain.* **2015**, *7* (8), 10461–10478. https://doi.org/10.3390/su70810461.

(3) Salem, K. S.; Naithani, V.; Jameel, H.; Lucia, L.; Pal, L. Lignocellulosic Fibers from Renewable Resources Using Green Chemistry for a Circular Economy. *Glob. Challenges* **2021**, *5* (2), 2000065. https://doi.org/https://doi.org/10.1002/gch2.202000065.

(4) Ciervo, M. Innovating for Sustainable Growth. A Bioeconomy for Europe. Un Punto Di Vista Geografico-Economico Critico. **2018**.

(5) Koelmans, A. A.; Gouin, T.; Thompson, R.; Wallace, N.; Arthur, C. Plastics in the Marine Environment. *Environ. Toxicol. Chem.* **2014**, *33* (1), 5–10. https://doi.org/https://doi.org/10.1002/etc.2426.

(6) Klemeš, J. J.; Fan, Y. V.; Jiang, P. Plastics: Friends or Foes? The Circularity and Plastic Waste Footprint. *Energy Sources, Part A Recover. Util. Environ. Eff.* **2020**, *00* (00), 1–17. https://doi.org/10.1080/15567036.2020.1801906.

(7) Weiss, M.; Haufe, J.; Carus, M.; Brandão, M.; Bringezu, S.; Hermann, B.; Patel, M. K. A Review of the Environmental Impacts of Biobased Materials. *J. Ind. Ecol.* **2012**, *16* (s1), S169–S181. https://doi.org/https://doi.org/10.1111/j.1530-9290.2012.00468.x.

(8) Kuczynski, J.; Boday, D. J. Bio-Based Materials for High-End Electronics Applications. *Int. J. Sustain. Dev. World Ecol.* **2012**, *19* (6), 557–563. https://doi.org/10.1080/13504509.2012.721404.

(9) Marriott, P. E.; Gómez, L. D.; McQueen-Mason, S. J. Unlocking the Potential of Lignocellulosic Biomass through Plant Science. *New Phytol.* **2016**, *209* (4), 1366–1381. https://doi.org/10.1111/nph.13684.

(10) Dahmen, N.; Lewandowski, I.; Zibek, S.; Weidtmann, A. Integrated Lignocellulosic Value Chains in a Growing Bioeconomy: Status Quo and Perspectives. *GCB Bioenergy* **2019**, *11* (1), 107–117. https://doi.org/https://doi.org/10.1111/gcbb.12586.

(11) Banwell, M. G.; Pollard, B.; Liu, X.; Connal, L. A. Exploiting Nature's Most Abundant Polymers: Developing New Pathways for the Conversion of Cellulose, Hemicellulose, Lignin and Chitin into Platform Molecules (and Beyond). *Chem. – An Asian J.* **2021**, *n/a* (n/a). https://doi.org/https://doi.org/10.1002/asia.202001451.

(12) Klemm, D.; Kramer, F.; Moritz, S.; Lindström, T.; Ankerfors, M.; Gray, D.; Dorris, A. Nanocelluloses: A New Family of Nature-Based Materials. *Angew. Chemie Int. Ed.* **2011**, *50* (24), 5438–5466. https://doi.org/https://doi.org/10.1002/anie.201001273.

(13) Dufresne, A. Nanocellulose Processing Properties and Potential Applications. *Curr. For. Reports* **2019**, 76–89. https://doi.org/10.1007/s40725-019-00088-1.

(14) Thomas, B.; Raj, M. C.; Athira, B. K.; Rubiyah, H. M.; Joy, J.; Moores, A.; Drisko, G. L.; Sanchez, C. Nanocellulose, a Versatile Green Platform: From Biosources to Materials and Their Applications. *Chem. Rev.* **2018**, *118* (24), 11575–11625. https://doi.org/10.1021/acs.chemrev.7b00627.

(15) Saito, T.; Kuramae, R.; Wohlert, J.; Berglund, L. A.; Isogai, A. An Ultrastrong Nanofibrillar Biomaterial: The Strength of Single Cellulose Nanofibrils Revealed via Sonication-Induced Fragmentation. *Biomacromolecules* **2013**, *14* (1), 248–253. https://doi.org/10.1021/bm301674e.

(16) Kim, D. W.; Shin, J.; Choi, S. Q. Nano-Dispersed Cellulose Nanofibrils-PMMA Composite from Pickering Emulsion with Tunable Interfacial Tensions. *Carbohydr. Polym.* **2020**, *247* (July). https://doi.org/10.1016/j.carbpol.2020.116762.

(17) Hasani, M.; Cranston, E. D.; Westman, G.; Gray, D. G. Cationic Surface Functionalization of Cellulose Nanocrystals. *Soft Matter* **2008**, *4* (11), 2238–2244. https://doi.org/10.1039/b806789a.

(18) Junior de Menezes, A.; Siqueira, G.; Curvelo, A. A. S.; Dufresne, A. Extrusion and Characterization of Functionalized Cellulose Whiskers Reinforced Polyethylene Nanocomposites. *Polymer (Guildf).* **2009**, *50* (19), 4552–4563. https://doi.org/https://doi.org/10.1016/j.polymer.2009.07.038.

(19) Yuan, H.; Nishiyama, Y.; Wada, M.; Kuga, S. Surface Acylation of Cellulose Whiskers by Drying Aqueous Emulsion. *Biomacromolecules* **2006**, *7* (3), 696–700. https://doi.org/10.1021/bm050828j.

(20) Raquez, J.-M.; Murena, Y.; Goffin, A.-L.; Habibi, Y.; Ruelle, B.; DeBuyl, F.; Dubois, P. Surface-Modification of Cellulose Nanowhiskers and Their Use as Nanoreinforcers into Polylactide: A Sustainably-Integrated Approach. *Compos. Sci. Technol.* **2012**, *72* (5), 544–549. https://doi.org/https://doi.org/10.1016/j.compscitech.2011.11.017.

(21) Robles, E.; Urruzola, I.; Labidi, J.; Serrano, L. Surface-Modified Nano-Cellulose as Reinforcement in Poly(Lactic Acid) to Conform New Composites. *Ind. Crops Prod.* **2015**, *71*, 44–53. https://doi.org/https://doi.org/10.1016/j.indcrop.2015.03.075.

(22) Abushammala, H.; Mao, J. A Review of the Surface Modification of Cellulose and Nanocellulose Using Aliphatic and Aromatic Mono- and Di-Isocyanates. *Molecules* . 2019. https://doi.org/10.3390/molecules24152782.

(23) Österberg, M.; Sipponen, M. H.; Mattos, B. D.; Rojas, O. J. Spherical Lignin Particles: A Review on Their Sustainability and Applications. *Green Chem.* **2020**, *22* (9), 2712–2733. https://doi.org/10.1039/d0gc00096e.

(24) Pang, T.; Wang, G.; Sun, H.; Wang, L.; Liu, Q.; Sui, W.; Parvez, A. M.; Si, C. Lignin Fractionation for Reduced Heterogeneity in Self-Assembly Nanosizing: Toward Targeted Preparation of Uniform Lignin Nanoparticles with Small Size. *ACS Sustain. Chem. Eng.* **2020**, *8* (24), 9174–9183. https://doi.org/10.1021/acssuschemeng.0c02967.

(25) Sipponen, M. H.; Lange, H.; Crestini, C.; Henn, A.; Österberg, M. Lignin for Nano- and Microscaled Carrier Systems: Applications, Trends, and Challenges. *ChemSusChem* **2019**, *12* (10), 2039–2054. https://doi.org/https://doi.org/10.1002/cssc.201900480.

(26) Bar-On, Y. M.; Phillips, R.; Milo, R. The Biomass Distribution on Earth. *Proc. Natl. Acad. Sci.* **2018**, *115* (25), 6506 LP – 6511. https://doi.org/10.1073/pnas.1711842115.

(27) Chen, C.; Kuang, Y.; Zhu, S.; Burgert, I.; Keplinger, T.; Gong, A.; Li, T.; Berglund, L.; Eichhorn, S. J.; Hu, L. Structure–Property–Function Relationships of Natural and Engineered Wood. *Nat. Rev. Mater.* **2020**, *5* (9), 642–666. https://doi.org/10.1038/s41578-020-0195-z.

(28) Pérez, J.; Muñoz-Dorado, J.; De La Rubia, T.; Martínez, J. Biodegradation and Biological Treatments of Cellulose, Hemicellulose and Lignin: An Overview. *Int. Microbiol.* **2002**, *5* (2), 53–63. https://doi.org/10.1007/s10123-002-0062-3.

(29) Rongpipi, S.; Ye, D.; Gomez, E. D.; Gomez, E. W. Progress and Opportunities in the Characterization of Cellulose – An Important Regulator of Cell Wall Growth and Mechanics . *Frontiers in Plant Science* . 2019, p 1894.

(30) Thomas, L. H.; Trevor Forsyth, V.; Šturcová, A.; Kennedy, C. J.; May, R. P.; Altaner, C. M.; Apperley, D. C.; Wess, T. J.; Jarvis, M. C. Structure of Cellulose Microfibrils in Primary Cell Walls from Collenchyma. *Plant Physiol.* **2013**, *161* (1), 465–476. https://doi.org/10.1104/pp.112.206359.
(31) Harris, D. M.; Corbin, K.; Wang, T.; Gutierrez, R.; Bertolo, A. L.; Petti, C.; Smilgies, D.-M. D.-M.; Estevez, J. M.; Bonetta, D.; Urbanowicz, B. R.; Ehrhardt, D. W.; Somerville, C. R.; Rose, J. K. C.; Hong, M.; DeBolt, S. Cellulose Microfibril Crystallinity Is Reduced by Mutating C-Terminal Transmembrane Region Residues CESA1A903V and CESA3T942I of Cellulose Synthase. *Proc. Natl. Acad. Sci.* **2012**, *109* (11), 4098–4103. https://doi.org/10.1073/pnas.1200352109.
(32) Balakshin, M.; Capanema, E. A.; Zhu, X.; Sulaeva, I.; Potthast, A.; Rosenau, T.; Rojas, O. J. Spruce Milled Wood Lignin: Linear, Branched or Cross-Linked? *Green Chem.* **2020**, *22* (13), 3985–4001. https://doi.org/10.1039/D0GC00926A.
(33) Crestini, C.; Lange, H.; Sette, M.; Argyropoulos, D. S. On the Structure of Softwood Kraft Lignin. *Green Chem.* **2017**, *19* (17), 4104–4121. https://doi.org/10.1039/C7GC01812F.
(34) Crestini, C.; Melone, F.; Sette, M.; Saladino, R. Milled Wood Lignin: A Linear Oligomer. *Biomacromolecules* **2011**, *12* (11), 3928–3935. https://doi.org/10.1021/bm200948r.
(35) Novaes, E.; Kirst, M.; Chiang, V.; Winter-Sederoff, H.; Sederoff, R. Lignin and Biomass: A Negative Correlation for Wood Formation and Lignin Content in Trees. *Plant Physiol.* **2010**, *154* (2), 555 LP – 561. https://doi.org/10.1104/pp.110.161281.
(36) Sajdak, M.; Lachowicz, H.; Wro, H. The Chemical Composition of Silver Birch (Betula Pendula Roth .) Wood in Poland Depending on Forest Stand Location and Forest Habitat Type. **2019**, *2*, 3047–3067. https://doi.org/10.1007/s10570-019-02306-2.
(37) Fre, B. H. Chemical Composition of Earlywood and Latewood in Norway Spruce Heartwood , Sapwood and Transition Zone Wood. **2004**, 245–256. https://doi.org/10.1007/s00226-004-0241-9.
(38) Allison, G. G.; Morris, C.; Lister, S. J.; Barraclough, T.; Yates, N.; Shield, I.; Donnison, I. S. Effect of Nitrogen Fertiliser Application on Cell Wall Composition in Switchgrass and Reed Canary Grass. *Biomass and Bioenergy* **2012**, *40*, 19–26. https://doi.org/10.1016/j.biombioe.2012.01.034.
(39) Wang, L.; Yang, M.; Fan, X.; Zhu, X.; Xu, T.; Yuan, Q. An Environmentally Friendly and Efficient Method for Xylitol Bioconversion with High-Temperature-Steaming Corncob Hydrolysate by Adapted Candida Tropicalis. *Process Biochem.* **2011**, *46* (8), 1619–1626. https://doi.org/10.1016/j.procbio.2011.05.004.
(40) O'Sullivan, A. C. Cellulose: The Structure Slowly Unravels. *Cellulose* **1997**, *4* (3), 173–207. https://doi.org/10.1023/A:1018431705579.
(41) Nishiyama, Y.; Langan, P.; Chanzy, H. Crystal Structure and Hydrogen-Bonding System in Cellulose Iβ from Synchrotron X-Ray and Neutron Fiber Diffraction. *J. Am. Chem. Soc.* **2002**, *124* (31), 9074–9082. https://doi.org/10.1021/ja0257319.
(42) Takahashi, Y.; Matsunaga, H. Crystal Structure of Native Cellulose. *Macromolecules* **1991**, *24* (13), 3968–3969. https://doi.org/10.1021/ma00013a035.
(43) Nishiyama, Y.; Sugiyama, J.; Chanzy, H.; Langan, P. Crystal Structure and Hydrogen Bonding System in Cellulose Iα from Synchrotron X-Ray and Neutron Fiber Diffraction. *J. Am. Chem. Soc.* **2003**, *125* (47), 14300–14306. https://doi.org/10.1021/ja037055w.
(44) Kovalenko, V. I. Crystalline Cellulose: Structure and Hydrogen Bonds. *Russ. Chem. Rev.* **2010**, *79* (3), 231–241. https://doi.org/10.1070/rc2010v079n03abeh004065.
(45) Nishiyama, Y. Structure and Properties of the Cellulose Microfibril. *J. Wood Sci.* **2009**, *55* (4), 241–249. https://doi.org/10.1007/s10086-009-1029-1.
(46) Kennedy, C. J.; Cameron, G. J.; Šturcová, A.; Apperley, D. C.; Altaner, C.; Wess,

T. J.; Jarvis, M. C. Microfibril Diameter in Celery Collenchyma Cellulose: X-Ray Scattering and NMR Evidence. *Cellulose* **2007**, *14* (3), 235. https://doi.org/10.1007/s10570-007-9116-1.

(47) Österberg, M.; Vartiainen, J.; Lucenius, J.; Hippi, U.; Seppälä, J.; Serimaa, R.; Laine, J.; Vartianen, J.; Lucenius, J.; Vartiainen, J.; Lucenius, J.; Hippi, U.; Seppälä, J.; Serimaa, R.; Laine, J. A Fast Method to Produce String NFC Films as a Platform for Barrier and Functional Materials. *ACS Appl. Mater. Interfaces* **2013**, *5* (11), 4640–4647. https://doi.org/10.1021/am401046x.

(48) Nishiyama, Y.; Kim, U.-J.; Kim, D.-Y.; Katsumata, K. S.; May, R. P.; Langan, P. Periodic Disorder along Ramie Cellulose Microfibrils. *Biomacromolecules* **2003**, *4* (4), 1013–1017. https://doi.org/10.1021/bm025772x.

(49) Okita, Y.; Saito, T.; Isogai, A. Entire Surface Oxidation of Various Cellulose Microfibrils by TEMPO-Mediated Oxidation. *Biomacromolecules* **2010**, *11* (6), 1696–1700. https://doi.org/10.1021/bm100214b.

(50) Ding, S.-Y.; Himmel, M. E. The Maize Primary Cell Wall Microfibril: A New Model Derived from Direct Visualization. *J. Agric. Food Chem.* **2006**, *54* (3), 597–606. https://doi.org/10.1021/jf051851z.

(51) Fernandes, A. N.; Thomas, L. H.; Altaner, C. M.; Callow, P.; Forsyth, V. T.; Apperley, D. C.; Kennedy, C. J.; Jarvis, M. C. Nanostructure of Cellulose Microfibrils in Spruce Wood. *Proc. Natl. Acad. Sci.* **2011**, *108* (47), 18863 LP – 18864.

(52) Oehme, D. P.; Downton, M. T.; Doblin, M. S.; Wagner, J.; Gidley, M. J.; Bacic, A. Unique Aspects of the Structure and Dynamics of Elementary I<Em>B</Em> Cellulose Microfibrils Revealed by Computational Simulations. *Plant Physiol.* **2015**, *168* (1), 3 LP – 17. https://doi.org/10.1104/pp.114.254664.

(53) Heise, K.; Kontturi, E.; Allahverdiyeva, Y.; Tammelin, T.; Linder, M. B.; Nonappa; Ikkala, O. Nanocellulose: Recent Fundamental Advances and Emerging Biological and Biomimicking Applications. *Adv. Mater.* **2021**, *33* (3), 2004349. https://doi.org/https://doi.org/10.1002/adma.202004349.

(54) Klemm, D.; Heublein, B.; Fink, H.-P.; Bohn, A. Cellulose: Fascinating Biopolymer and Sustainable Raw Material. *Angew. Chemie Int. Ed.* **2005**, *44* (22), 3358–3393. https://doi.org/https://doi.org/10.1002/anie.200460587.

(55) Youssefian, S.; Rahbar, N. Molecular Origin of Strength and Stiffness in Bamboo Fibrils. *Sci. Rep.* **2015**, *5* (1), 11116. https://doi.org/10.1038/srep11116.

(56) Isogai, A.; Saito, T.; Fukuzumi, H. TEMPO-Oxidized Cellulose Nanofibers. *Nanoscale* **2011**, *3* (1), 71–85. https://doi.org/10.1039/C0NR00583E.

(57) Boldizar, A.; Klason, C.; Kubát, J.; Näslund, P.; Sáha, P. Prehydrolyzed Cellulose as Reinforcing Filler for Thermoplastics. *Int. J. Polym. Mater. Polym. Biomater.* **1987**, *11* (4), 229–262. https://doi.org/10.1080/00914038708078665.

(58) Pääkko, M.; Ankerfors, M.; Kosonen, H.; Nykänen, A.; Ahola, S.; Österberg, M.; Ruokolainen, J.; Laine, J.; Larsson, P. T. T.; Ikkala, O.; Lindström, T.; Pääkkö, M.; Ankerfors, M.; Kosonen, H.; Nykänen, A.; Ahola, S.; Österberg, M.; Ruokolainen, J.; Laine, J.; Larsson, P. T. T.; Ikkala, O.; Lindström, T. Enzymatic Hydrolysis Combined with Mechanical Shearing and High-Pressure Homogenization for Nanoscale Cellulose Fibrils and Strong Gels. *Biomacromolecules* **2007**, *8* (6), 1934–1941. https://doi.org/10.1021/bm061215p.

(59) Henriksson, M.; Henriksson, G.; Berglund, L. A.; Lindström, T. An Environmentally Friendly Method for Enzyme-Assisted Preparation of Microfibrillated Cellulose (MFC) Nanofibers. *Eur. Polym. J.* **2007**, *43* (8), 3434–3441. https://doi.org/https://doi.org/10.1016/j.eurpolymj.2007.05.038.

(60) Wågberg, L.; Decher, G.; Norgren, M.; Lindström, T.; Ankerfors, M.; Axnäs, K. The Build-Up of Polyelectrolyte Multilayers of Microfibrillated Cellulose and Cationic Polyelectrolytes. *Langmuir* **2008**, *24* (3), 784–795. https://doi.org/10.1021/la702481v.

(61) Ansari, F.; Berglund, L. A. Chapter 4 - Tensile Properties of Wood Cellulose Nanopaper and Nanocomposite Films; Puglia, D., Fortunati, E., Kenny, J. M. B.

T.-M. P. N. B. on C. R., Eds.; William Andrew Publishing, 2016; pp 115–130. https://doi.org/https://doi.org/10.1016/B978-0-323-44248-0.00004-3.
(62) Yousuf, A.; Pirozzi, D.; Sannino, F. Chapter 1 - Fundamentals of Lignocellulosic Biomass; Yousuf, A., Pirozzi, D., Sannino, F. B. T.-L. B. to L. B., Eds.; Academic Press, 2020; pp 1–15. https://doi.org/https://doi.org/10.1016/B978-0-12-815936-1.00001-0.
(63) Lu, Y.; Lu, Y.-C.; Hu, H.-Q.; Xie, F.-J.; Wei, X.-Y.; Fan, X. Structural Characterization of Lignin and Its Degradation Products with Spectroscopic Methods. *J. Spectrosc.* **2017**, *2017*, 8951658. https://doi.org/10.1155/2017/8951658.
(64) Sarkar, P.; Bosneaga, E.; Auer, M. Plant Cell Walls throughout Evolution: Towards a Molecular Understanding of Their Design Principles. *J. Exp. Bot.* **2009**, *60* (13), 3615–3635. https://doi.org/10.1093/jxb/erp245.
(65) Meng, X.; Crestini, C.; Ben, H.; Hao, N.; Pu, Y.; Ragauskas, A. J.; Argyropoulos, D. S. Determination of Hydroxyl Groups in Biorefinery Resources via Quantitative 31P NMR Spectroscopy. *Nat. Protoc.* **2019**, *14* (9), 2627–2647. https://doi.org/10.1038/s41596-019-0191-1.
(66) Kai, D.; Tan, M. J.; Chee, P. L.; Chua, Y. K.; Yap, Y. L.; Loh, X. J. Towards Lignin-Based Functional Materials in a Sustainable World. *Green Chem.* **2016**, *18* (5), 1175–1200. https://doi.org/10.1039/c5gc02616d.
(67) Becker, J.; Wittmann, C. A Field of Dreams: Lignin Valorization into Chemicals, Materials, Fuels, and Health-Care Products. *Biotechnol. Adv.* **2019**, *37* (6), 107360. https://doi.org/https://doi.org/10.1016/j.biotechadv.2019.02.016.
(68) Bruijnincx, P. C. A.; Weckhuysen, B. M. Lignin up for Break-Down. *Nat. Chem.* **2014**, *6* (12), 1035–1036. https://doi.org/10.1038/nchem.2120.
(69) Beckham, G. T.; Johnson, C. W.; Karp, E. M.; Salvachu, D. ScienceDirect Opportunities and Challenges in Biological Lignin Valorization ´ a and Derek R Vardon Biological Valorization of Lignin to Chemicals. **2016**, No. March, 40–53. https://doi.org/10.1016/j.copbio.2016.02.030.
(70) Figueiredo, P.; Ferro, C.; Kemell, M.; Liu, Z.; Kiriazis, A.; Lintinen, K.; Florindo, H. F.; Yli-Kauhaluoma, J.; Hirvonen, J.; Kostiainen, M. A.; Santos, H. A. Functionalization of Carboxylated Lignin Nanoparticles for Targeted and PH-Responsive Delivery of Anticancer Drugs. *Nanomedicine* **2017**, *12* (21), 2581–2596. https://doi.org/10.2217/nnm-2017-0219.
(71) Figueiredo, P.; Sipponen, M. H.; Lintinen, K.; Correia, A.; Kiriazis, A.; Yli-Kauhaluoma, J.; Österberg, M.; George, A.; Hirvonen, J.; Kostiainen, M. A.; Santos, H. A. Preparation and Characterization of Dentin Phosphophoryn-Derived Peptide-Functionalized Lignin Nanoparticles for Enhanced Cellular Uptake. *Small* **2019**, *15* (24), 1–14. https://doi.org/10.1002/smll.201901427.
(72) Qian, Y.; Deng, Y.; Qiu, X.; Li, H.; Yang, D. Formation of Uniform Colloidal Spheres from Lignin, a Renewable Resource Recovered from Pulping Spent Liquor. *Green Chem.* **2014**, *16* (4), 2156–2163. https://doi.org/10.1039/c3gc42131g.
(73) Lievonen, M.; Valle-Delgado, J. J.; Mattinen, M.-L. L.; Hult, E.-L. L.; Lintinen, K.; Kostiainen, M. A.; Paananen, A.; Szilvay, G. R.; Setälä, H.; Österberg, M. A Simple Process for Lignin Nanoparticle Preparation. *Green Chem.* **2016**, *18* (5), 1416–1422. https://doi.org/10.1039/c5gc01436k.
(74) Mattinen, M. L.; Riviere, G.; Henn, A.; Nugroho, R. W. N.; Leskinen, T.; Nivala, O.; Valle-Delgado, J. J.; Kostiainen, M. A.; Österberg, M. Colloidal Lignin Particles as Adhesives for Soft Materials. *Nanomaterials* **2018**, *8* (12). https://doi.org/10.3390/nano8121001.
(75) Richter, A. P.; Bharti, B.; Armstrong, H. B.; Brown, J. S.; Plemmons, D.; Paunov, V. N.; Stoyanov, S. D.; Velev, O. D. Synthesis and Characterization of Biodegradable Lignin Nanoparticles with Tunable Surface Properties. *Langmuir* **2016**, *32* (25), 6468–6477. https://doi.org/10.1021/acs.langmuir.6b01088.
(76) Yang, W.; Dominici, F.; Fortunati, E.; Kenny, J. M.; Puglia, D. Effect of Lignin Nanoparticles and Masterbatch Procedures on the Final Properties of Glycidyl Methacrylate-g-Poly (Lactic Acid) Films before and after Accelerated UV

Weathering. *Ind. Crops Prod.* **2015**, *77*, 833–844. https://doi.org/10.1016/j.indcrop.2015.09.057.
(77) Sipponen, M. H. M. H. M. H.; Lange, H.; Ago, M.; Crestini, C. Understanding Lignin Aggregation Processes. A Case Study: Budesonide Entrapment and Stimuli Controlled Release from Lignin Nanoparticles. *ACS Sustain. Chem. Eng.* **2018**, *6* (7), 9342–9351. https://doi.org/10.1021/acssuschemeng.8b01652.
(78) Myint, A. A.; Lee, H. W.; Seo, B.; Son, W. S.; Yoon, J. J.; Yoon, T. J.; Park, H. J.; Yu, J.; Yoon, J. J.; Lee, Y. W. One Pot Synthesis of Environmentally Friendly Lignin Nanoparticles with Compressed Liquid Carbon Dioxide as an Antisolvent. *Green Chem.* **2016**, *18* (7), 2129–2146. https://doi.org/10.1039/c5gc02398j.
(79) Ago, M.; Huan, S.; Borghei, M.; Raula, J.; Kauppinen, E. I.; Rojas, O. J. High-Throughput Synthesis of Lignin Particles (~30 Nm to ~2 Mm) via Aerosol Flow Reactor: Size Fractionation and Utilization in Pickering Emulsions. *ACS Appl. Mater. Interfaces* **2016**, *8* (35), 23302–23310. https://doi.org/10.1021/acsami.6b07900.
(80) Zhou, Y.; Qian, Y.; Wu, S.; Zhong, X.; Huang, J.; Qiu, X. Incorporation of Nano Lignin Reverse Micelles on the Transparency, UV-Blocking and Rheological Properties of High-Density Polyethylene Films. *Holzforschung* **2019**. https://doi.org/10.1515/hf-2019-0091.
(81) Ma, M.; Dai, L.; Xu, J.; Liu, Z.; Ni, Y. A Simple and Effective Approach to Fabricate Lignin Nanoparticles with Tunable Sizes Based on Lignin Fractionation. *Green Chem.* **2020**, *22* (6), 2011–2017. https://doi.org/10.1039/d0gc00377h.
(82) Tian, D.; Hu, J.; Bao, J.; Chandra, R. P.; Saddler, J. N.; Lu, C. Lignin Valorization: Lignin Nanoparticles as High-Value Bio-Additive for Multifunctional Nanocomposites. *Biotechnol. Biofuels* **2017**, *10* (1), 1–11. https://doi.org/10.1186/s13068-017-0876-z.
(83) Zou, T.; Sipponen, M. H.; Österberg, M. Natural Shape-Retaining Microcapsules with Shells Made of Chitosan-Coated Colloidal Lignin Particles. *Front. Chem.* **2019**, *7* (MAY), 1–12. https://doi.org/10.3389/fchem.2019.00370.
(84) Frangville, C.; Rutkevičius, M.; Richter, A. P.; Velev, O. D.; Stoyanov, S. D.; Paunov, V. N. Fabrication of Environmentally Biodegradable Lignin Nanoparticles. *ChemPhysChem* **2012**, *13* (18), 4235–4243. https://doi.org/10.1002/cphc.201200537.
(85) Cusola, O.; Kivistö, S.; Vierros, S.; Batys, P.; Ago, M.; Tardy, B. L.; Greca, L. G.; Roncero, M. B.; Sammalkorpi, M.; Rojas, O. J. Particulate Coatings via Evaporation-Induced Self-Assembly of Polydisperse Colloidal Lignin on Solid Interfaces. *Langmuir* **2018**, *34* (20), 5759–5771. https://doi.org/10.1021/acs.langmuir.8b00650.
(86) Gilca, I. A.; Popa, V. I.; Crestini, C. Obtaining Lignin Nanoparticles by Sonication. *Ultrason. Sonochem.* **2015**, *23*, 369–375. https://doi.org/10.1016/j.ultsonch.2014.08.021.
(87) Sanyang, M. L.; Jawaid, M. *Bio-Based Polymers and Nanocomposites: Preparation, Processing, Properties & Performance*; Springer International Publishing, 2019.
(88) Sehaqui, H.; Zhou, Q.; Ikkala, O.; Berglund, L. A. Strong and Tough Cellulose Nanopaper with High Specific Surface Area and Porosity. *Biomacromolecules* **2011**, *12* (10), 3638–3644. https://doi.org/10.1021/bm2008907.
(89) Shen, R.; Xue, S.; Xu, Y.; Liu, Q.; Feng, Z.; Ren, H.; Zhai, H. Research Progress and Development Demand Of. **2020**, 1–19.
(90) Them, I. Recent Advances in Nanocellulose Composites with Polymers : A Guide for Choosing Partners and How To. **2018**. https://doi.org/10.3390/polym10050517.
(91) Sehaqui, H.; Zimmermann, T.; Tingaut, P. Hydrophobic Cellulose Nanopaper through a Mild Esterification Procedure. *Cellulose* **2014**, *21* (1), 367–382. https://doi.org/10.1007/s10570-013-0110-5.
(92) Leppänen, I.; Vikman, M.; Harlin, A.; Orelma, H. Enzymatic Degradation and

Pilot-Scale Composting of Cellulose-Based Films with Different Chemical Structures. *J. Polym. Environ.* **2020**, *28* (2), 458–470. https://doi.org/10.1007/s10924-019-01621-w.
(93) Yang, M.; Zhang, X.; Guan, S.; Dou, Y.; Gao, X.; Miao, L. Green Preparation of Lignin Nanoparticles in an Aqueous Hydrotropic Solution and Application in Biobased Nanocomposite Films. *Holzforschung* **2020**. https://doi.org/doi:10.1515/hf-2020-0021.
(94) Yang, W.; Fortunati, E.; Dominici, F.; Kenny, J. M.; Puglia, D. Effect of Processing Conditions and Lignin Content on Thermal, Mechanical and Degradative Behavior of Lignin Nanoparticles/Polylactic (Acid) Bionanocomposites Prepared by Melt Extrusion and Solvent Casting. *Eur. Polym. J.* **2015**, *71*, 126–139. https://doi.org/https://doi.org/10.1016/j.eurpolymj.2015.07.051.
(95) Pouteau, C.; Baumberger, S.; Cathala, B.; Dole, P. Lignin–Polymer Blends: Evaluation of Compatibility by Image Analysis. *C. R. Biol.* **2004**, *327* (9), 935–943. https://doi.org/https://doi.org/10.1016/j.crvi.2004.08.008.
(96) Yang, W.; Owczarek, J. S.; Fortunati, E.; Kozanecki, M.; Mazzaglia, A.; Balestra, G. M.; Kenny, J. M.; Torre, L.; Puglia, D. Antioxidant and Antibacterial Lignin Nanoparticles in Polyvinyl Alcohol/Chitosan Films for Active Packaging. *Ind. Crops Prod.* **2016**, *94*, 800–811. https://doi.org/10.1016/j.indcrop.2016.09.061.
(97) Zhang, X.; Liu, W.; Liu, W.; Qiu, X. High Performance PVA/Lignin Nanocomposite Films with Excellent Water Vapor Barrier and UV-Shielding Properties. *Int. J. Biol. Macromol.* **2020**, *142*, 551–558. https://doi.org/https://doi.org/10.1016/j.ijbiomac.2019.09.129.
(98) Ju, T.; Zhang, Z.; Li, Y.; Miao, X.; Ji, J. Continuous Production of Lignin Nanoparticles Using a Microchannel Reactor and Its Application in UV-Shielding Films. *RSC Adv.* **2019**, *9* (43), 24915–24921. https://doi.org/10.1039/C9RA05064G.
(99) Yang, W.; Kenny, J. M.; Puglia, D. Structure and Properties of Biodegradable Wheat Gluten Bionanocomposites Containing Lignin Nanoparticles. *Ind. Crops Prod.* **2015**, *74*, 348–356. https://doi.org/10.1016/j.indcrop.2015.05.032.
(100) Yang, W.; Fortunati, E.; Dominici, F.; Giovanale, G.; Mazzaglia, A.; Balestra, G. M.; Kenny, J. M.; Puglia, D. Synergic Effect of Cellulose and Lignin Nanostructures in PLA Based Systems for Food Antibacterial Packaging. *Eur. Polym. J.* **2016**, *79*, 1–12. https://doi.org/10.1016/j.eurpolymj.2016.04.003.
(101) Moreno, A.; Sipponen, M. H. Biocatalytic Nanoparticles for the Stabilization of Degassed Single Electron Transfer-Living Radical Pickering Emulsion Polymerizations. *Nat. Commun.* **2020**, *11* (1), 5599. https://doi.org/10.1038/s41467-020-19407-3.
(102) Dai, L.; Liu, R.; Hu, L.-Q.; Zou, Z.-F.; Si, C.-L. Resveratrol. *ACS Sustain. Chem. Eng.* **2017**, *5* (9), 8241–8249. https://doi.org/10.1021/acssuschemeng.7b01903.
(103) Figueiredo, P.; Lintinen, K.; Kiriazis, A.; Hynninen, V.; Liu, Z.; Bauleth-Ramos, T.; Rahikkala, A.; Correia, A.; Kohout, T.; Sarmento, B.; Yli-Kauhaluoma, J.; Hirvonen, J.; Ikkala, O.; Kostiainen, M. A.; Santos, H. A. In Vitro Evaluation of Biodegradable Lignin-Based Nanoparticles for Drug Delivery and Enhanced Antiproliferation Effect in Cancer Cells. *Biomaterials* **2017**, *121*, 97–108. https://doi.org/https://doi.org/10.1016/j.biomaterials.2016.12.034.
(104) Alqahtani, M. S.; Alqahtani, A.; Al-Thabit, A.; Roni, M.; Syed, R. Novel Lignin Nanoparticles for Oral Drug Delivery. *J. Mater. Chem. B* **2019**, *7* (28), 4461–4473. https://doi.org/10.1039/C9TB00594C.
(105) Wang, M.; Yang, D.; Xu, Q.; Li, P.; Yi, C.; Qian, Y.; Qiu, X. Highly Efficient Evaporation Method to Prepare PH-Responsive Lignin-Hollow-Nanosphere with Controllable Size and Its Application in Oral Drug Delivery. *Ind. Crops Prod.* **2021**, *162*, 113230. https://doi.org/https://doi.org/10.1016/j.indcrop.2020.113230.
(106) Machado, T. O.; Beckers, S. J.; Fischer, J.; Müller, B.; Sayer, C.; de Araújo, P. H. H.; Landfester, K.; Wurm, F. R. Bio-Based Lignin Nanocarriers Loaded with Fungicides as a Versatile Platform for Drug Delivery in Plants.

Biomacromolecules **2020**, *21* (7), 2755–2763. https://doi.org/10.1021/acs.biomac.0c00487.
(107) Sipponen, M. H.; Henn, A.; Penttilä, P.; Österberg, M. Lignin-Fatty Acid Hybrid Nanocapsules for Scalable Thermal Energy Storage in Phase-Change Materials. *Chem. Eng. J.* **2020**, *393* (February), 124711. https://doi.org/https://doi.org/10.1016/j.cej.2020.124711.
(108) Sipponen, M. H.; Farooq, M.; Koivisto, J.; Pellis, A.; Seitsonen, J.; Österberg, M. Spatially Confined Lignin Nanospheres for Biocatalytic Ester Synthesis in Aqueous Media. *Nat. Commun.* **2018**, *9*, 1–7. https://doi.org/10.1038/s41467-018-04715-6.
(109) Lavoine, N.; Bergström, L. Nanocellulose-Based Foams and Aerogels: Processing, Properties, and Applications. *J. Mater. Chem. A* **2017**, *5* (31), 16105–16117. https://doi.org/10.1039/c7ta02807e.
(110) De France, K. J.; Hoare, T.; Cranston, E. D. Review of Hydrogels and Aerogels Containing Nanocellulose. *Chem. Mater.* **2017**, *29* (11), 4609–4631. https://doi.org/10.1021/acs.chemmater.7b00531.
(111) Costes, L.; Laoutid, F.; Brohez, S.; Dubois, P. Bio-Based Flame Retardants: When Nature Meets Fire Protection. *Mater. Sci. Eng. R Reports* **2017**, *117*, 1–25. https://doi.org/https://doi.org/10.1016/j.mser.2017.04.001.
(112) Guo, L.; Chen, Z.; Lyu, S.; Fu, F.; Wang, S. Highly Flexible Cross-Linked Cellulose Nanofibril Sponge-like Aerogels with Improved Mechanical Property and Enhanced Flame Retardancy. *Carbohydr. Polym.* **2018**, *179* (September 2017), 333–340. https://doi.org/https://doi.org/10.1016/j.carbpol.2017.09.084.
(113) Guo, W.; Wang, X.; Zhang, P.; Liu, J.; Song, L.; Hu, Y. Nano-Fibrillated Cellulose-Hydroxyapatite Based Composite Foams with Excellent Fire Resistance. *Carbohydr. Polym.* **2018**, *195* (March), 71–78. https://doi.org/https://doi.org/10.1016/j.carbpol.2018.04.063.
(114) Luo, X.; Shen, J.; Ma, Y.; Liu, L.; Meng, R.; Yao, J. Robust, Sustainable Cellulose Composite Aerogels with Outstanding Flame Retardancy and Thermal Insulation. *Carbohydr. Polym.* **2020**, *230*, 115623. https://doi.org/https://doi.org/10.1016/j.carbpol.2019.115623.
(115) Wang, L.; Sánchez-Soto, M.; Fan, J.; Xia, Z.-P.; Liu, Y. Boron/Nitrogen Flame Retardant Additives Cross-Linked Cellulose Nanofibril/Montmorillonite Aerogels toward Super-Low Flammability and Improved Mechanical Properties. *Polym. Adv. Technol.* **2019**, *30* (7), 1807–1817. https://doi.org/https://doi.org/10.1002/pat.4613.
(116) Farooq, M.; Sipponen, M. H.; Seppälä, A.; Österberg, M. Eco-Friendly Flame-Retardant Cellulose Nanofibril Aerogels by Incorporating Sodium Bicarbonate. *ACS Appl. Mater. Interfaces* **2018**, *10* (32), 27407–27415. https://doi.org/10.1021/acsami.8b04376.
(117) Swerin, A.; Odberg, L.; Lindström, T. Deswelling of Hardwood Kraft Pulp Fibers by Cationic Polymers. *Nord. Pulp Pap. Res. J.* **1990**, *5* (4), 188–196. https://doi.org/doi:10.3183/npprj-1990-05-04-p188-196.
(118) Sipponen, M. H.; Smyth, M.; Leskinen, T.; Johansson, L.-S.; Österberg, M. All-Lignin Approach to Prepare Cationic Colloidal Lignin Particles: Stabilization of Durable Pickering Emulsions. *Green Chem.* **2017**, *19* (24), 5831–5840. https://doi.org/10.1039/C7GC02900D.
(119) Choi, J.-H. H.; Kim, S.-O. O.; Linardy, E.; Dreaden, E. C.; Zhdanov, V. P.; Hammond, P. T.; Cho, N.-J. J. Influence of PH and Surface Chemistry on Poly(l-Lysine) Adsorption onto Solid Supports Investigated by Quartz Crystal Microbalance with Dissipation Monitoring. *J. Phys. Chem. B* **2015**, *119* (33), 10554–10565. https://doi.org/10.1021/acs.jpcb.5b01553.
(120) Liu, H.; Cao, G. Effectiveness of the Young-Laplace Equation at Nanoscale. *Sci. Rep.* **2016**, *6* (1), 23936. https://doi.org/10.1038/srep23936.
(121) Park, S.; Venditti, R. A.; Jameel, H.; Pawlak, J. J. Changes in Pore Size Distribution during the Drying of Cellulose Fibers as Measured by Differential Scanning Calorimetry. *Carbohydr. Polym.* **2006**, *66* (1), 97–103. https://doi.org/10.1016/j.carbpol.2006.02.026.
(122) Pihlajaniemi, V.; Sipponen, M. H.; Liimatainen, H.; Sirviö, J. A.; Nyyssölä, A.;

Laakso, S. Weighing the Factors behind Enzymatic Hydrolyzability of Pretreated Lignocellulose. *Green Chem.* **2016**, *18*, 1295–1305. https://doi.org/10.1039/C5GC01861G.
(123) Bakirtzis, D.; Delichatsios, M. A.; Liodakis, S.; Ahmed, W. Fire Retardancy Impact of Sodium Bicarbonate on Ligno-Cellulosic Materials. *Thermochim. Acta* **2009**, *486* (1), 11–19. https://doi.org/https://doi.org/10.1016/j.tca.2008.12.012.
(124) Bakirtzis, D. S.; Tsapara, V. C.; Kolovos, K. G.; Liodakis, S. E. Assessment of the Impact of Fire Retardants on the Combustion of Natural Polymers Employing DTG and LOI. *Fire Mater.* **2015**, *39* (2), 109–118. https://doi.org/https://doi.org/10.1002/fam.2232.
(125) Carosio, F.; Kochumalayil, J.; Cuttica, F.; Camino, G.; Berglund, L. Oriented Clay Nanopaper from Biobased Components - Mechanisms for Superior Fire Protection Properties. *ACS Appl. Mater. Interfaces* **2015**, *7* (10), 5847–5856. https://doi.org/10.1021/am509058h.
(126) Guo, W.; Hu, Y.; Wang, X.; Zhang, P.; Song, L.; Xing, W. Exceptional Flame-Retardant Cellulosic Foams Modified with Phosphorus-Hybridized Graphene Nanosheets. *Cellulose* **2019**, *26* (2), 1247–1260. https://doi.org/10.1007/s10570-018-2127-2.
(127) Kovbasyuk, L.; Mokhir, A.; Lowe, S. E.; Zhong, Y. L. Toxicity Studies and Biomedical Applications of Graphene Oxide. *Graphene Oxide*. October 13, 2016, pp 364–381. https://doi.org/https://doi.org/10.1002/9781119069447.ch11.
(128) Yang, L.; Mukhopadhyay, A.; Jiao, Y.; Yong, Q.; Chen, L.; Xing, Y.; Hamel, J.; Zhu, H. Ultralight, Highly Thermally Insulating and Fire Resistant Aerogel by Encapsulating Cellulose Nanofibers with Two-Dimensional MoS2. *Nanoscale* **2017**, *9* (32), 11452–11462. https://doi.org/10.1039/c7nr02243c.
(129) Li, Y.; Wang, B.; Sui, X.; Xu, H.; Zhang, L.; Zhong, Y.; Mao, Z. Facile Synthesis of Microfibrillated Cellulose/Organosilicon/Polydopamine Composite Sponges with Flame Retardant Properties. *Cellulose* **2017**, *24* (9), 3815–3823. https://doi.org/10.1007/s10570-017-1373-z.
(130) Ash, M. *Handbook of Fillers, Extenders, and Diluents. Synapse Info Resources*; 2007; Vol. 53.
(131) Zhao, M. Potential Estrogenic E Ff Ects of Phosphorus-Containing Flame Retardants. **2014**.
(132) Mohsin, M.; Ahmad, S. W.; Khatri, A.; Zahid, B. Performance Enhancement of Fire Retardant Finish with Environment Friendly Bio Cross-Linker for Cotton. *J. Clean. Prod.* **2013**, *51*, 191–195. https://doi.org/10.1016/j.jclepro.2013.01.031.
(133) Du, J.; Li, H.; Xu, S.; Zhou, Q.; Jin, M.; Tang, J. A Review of Organophosphorus Flame Retardants (OPFRs): Occurrence, Bioaccumulation, Toxicity, and Organism Exposure. *Environ. Sci. Pollut. Res.* **2019**, *26* (22), 22126–22136. https://doi.org/10.1007/s11356-019-05669-y.
(134) Zheng, C.; Li, D.; Ek, M. Improving Fire Retardancy of Cellulosic Thermal Insulating Materials by Coating with Bio-Based Fire Retardants. *Nord. Pulp Pap. Res. J.* **2019**, *34* (1), 96–106. https://doi.org/10.1515/npprj-2018-0031.
(135) Long, L.-Y.; Weng, Y.-X.; Wang, Y.-Z. Cellulose Aerogels: Synthesis, Applications, and Prospects. *Polymers (Basel).* **2018**, *10* (6), 623. https://doi.org/10.3390/polym10060623.
(136) Kunič, R. Forest-Based Bioproducts Used for Construction and Its Impact on the Environmental Performance of a Building in the Whole Life Cycle BT - Environmental Impacts of Traditional and Innovative Forest-Based Bioproducts; Kutnar, A., Muthu, S. S., Eds.; Springer Singapore: Singapore, 2016; pp 173–204. https://doi.org/10.1007/978-981-10-0655-5_5.
(137) Larkin, P. *Infrared and Raman Spectroscopy: Principles and Spectral Interpretation*; Elsevier Science, 2017.
(138) Xiong, F.; Han, Y.; Wang, S.; Li, G.; Qin, T.; Chen, Y.; Chu, F. Preparation and Formation Mechanism of Renewable Lignin Hollow Nanospheres with a Single Hole by Self-Assembly. *ACS Sustain. Chem. Eng.* **2017**, *5* (3), 2273–2281. https://doi.org/10.1021/acssuschemeng.6b02585.

(139) Liu, Z.; Hao, N.; Shinde, S.; Pu, Y.; Kang, X.; Ragauskas, A. J.; Yuan, J. S. Tailored Lignin Reactivity by Sequential Organosolv. **2018**. https://doi.org/10.1039/c8gc03290d.
(140) Tian, D.; Hu, J.; Chandra, R. P.; Saddler, J. N.; Lu, C. Valorizing Recalcitrant Cellulolytic Enzyme Lignin via Lignin Nanoparticles Fabrication in an Integrated Biore Fi Nery. **2017**. https://doi.org/10.1021/acssuschemeng.6b03043.
(141) Zou, T.; Sipponen, M. H.; Henn, A.; Österberg, M. Solvent-Resistant Lignin-Epoxy Hybrid Nanoparticles for Covalent Surface Modification and High-Strength Particulate Adhesives. *ACS Nano* **2021**. https://doi.org/10.1021/acsnano.0c09500.
(142) Farooq, M.; Zou, T.; Riviere, G.; Sipponen, M. H.; Österberg, M. Strong, Ductile, and Waterproof Cellulose Nanofibril Composite Films with Colloidal Lignin Particles. *Biomacromolecules* **2019**, *20* (2), 693–704. https://doi.org/10.1021/acs.biomac.8b01364.
(143) Peng, Y.; Gardner, D. J.; Han, Y.; Kiziltas, A.; Cai, Z.; Tshabalala, M. A. Influence of Drying Method on the Material Properties of Nanocellulose I: Thermostability and Crystallinity. *Cellulose* **2013**, *20* (5), 2379–2392. https://doi.org/10.1007/s10570-013-0019-z.
(144) Sinquefield, S.; Ciesielski, P. N.; Li, K.; Gardner, D. J.; Ozcan, S. Nanocellulose Dewatering and Drying: Current State and Future Perspectives. *ACS Sustain. Chem. Eng.* **2020**, *8* (26), 9601–9615. https://doi.org/10.1021/acssuschemeng.0c01797.
(145) Noor Mohamed, N. H.; Takagi, H.; Nakagaito, A. N. Mechanical Properties of Heat-Treated Cellulose Nanofiber-Reinforced Polyvinyl Alcohol Nanocomposite. *J. Compos. Mater.* **2016**, *51* (14), 1971–1977. https://doi.org/10.1177/0021998316665238.
(146) Walther, A.; Lossada, F.; Benselfelt, T.; Kriechbaum, K.; Berglund, L.; Ikkala, O.; Saito, T.; Wågberg, L.; Bergström, L. Best Practice for Reporting Wet Mechanical Properties of Nanocellulose-Based Materials. *Biomacromolecules* **2020**, *21* (6), 2536–2540. https://doi.org/10.1021/acs.biomac.0c00330.
(147) Malho, J.-M.; Ouellet-Plamondon, C.; Rüggeberg, M.; Laaksonen, P.; Ikkala, O.; Burgert, I.; Linder, M. B. Enhanced Plastic Deformations of Nanofibrillated Cellulose Film by Adsorbed Moisture and Protein-Mediated Interactions. *Biomacromolecules* **2015**, *16* (1), 311–318. https://doi.org/10.1021/bm501514w.
(148) Ding, Q.; Zeng, J.; Wang, B.; Tang, D.; Chen, K.; Gao, W. Effect of Nanocellulose Fiber Hornification on Water Fraction Characteristics and Hydroxyl Accessibility during Dehydration. *Carbohydr. Polym.* **2019**, *207*, 44–51. https://doi.org/https://doi.org/10.1016/j.carbpol.2018.11.075.
(149) Henriksson, M.; Berglund, L. A.; Isaksson, P.; Lindström, T.; Nishino, T. Cellulose Nanopaper Structures of High Toughness. *Biomacromolecules* **2008**, *9* (6), 1579–1585. https://doi.org/10.1021/bm800038n.
(150) Zhu, H.; Zhu, S.; Jia, Z.; Parvinian, S.; Li, Y.; Vaaland, O.; Hu, L.; Li, T. Anomalous Scaling Law of Strength and Toughness of Cellulose Nanopaper. *Proc. Natl. Acad. Sci. U. S. A.* **2015**, *112* (29), 8971–8976. https://doi.org/10.1073/pnas.1502870112.
(151) Wang, Q.; Du, H.; Zhang, F.; Zhang, Y.; Wu, M.; Yu, G.; Liu, C.; Li, B.; Peng, H. Flexible Cellulose Nanopaper with High Wet Tensile Strength, High Toughness and Tunable Ultraviolet Blocking Ability Fabricated from Tobacco Stalk: Via a Sustainable Method. *J. Mater. Chem. A* **2018**, *6* (27), 13021–13030. https://doi.org/10.1039/c8ta01986j.
(152) Herrera, M.; Thitiwutthisakul, K.; Yang, X.; Rujitanaroj, P. on; Rojas, R.; Berglund, L. Preparation and Evaluation of High-Lignin Content Cellulose Nanofibrils from Eucalyptus Pulp. *Cellulose* **2018**, *25* (5), 3121–3133. https://doi.org/10.1007/s10570-018-1764-9.
(153) Rojo, E.; Peresin, M. S.; Sampson, W. W.; Hoeger, I. C.; Vartiainen, J.; Laine, J.; Rojas, O. J. Comprehensive Elucidation of the Effect of Residual Lignin on the Physical, Barrier, Mechanical and Surface Properties of Nanocellulose Films. *Green Chem.* **2015**, *17* (3), 1853–1866.

https://doi.org/10.1039/c4gc02398f.
(154) Bian, H.; Gao, Y.; Wang, R.; Liu, Z.; Wu, W.; Dai, H. Contribution of Lignin to the Surface Structure and Physical Performance of Cellulose Nanofibrils Film. *Cellulose* **2018**, *25* (2), 1309–1318. https://doi.org/10.1007/s10570-018-1658-x.
(155) Kutvonen, A.; Rossi, G.; Puisto, S. R.; Rostedt, N. K. J.; Ala-Nissila, T. Influence of Nanoparticle Size, Loading, and Shape on the Mechanical Properties of Polymer Nanocomposites. *J. Chem. Phys.* **2012**, *137* (21), 214901. https://doi.org/10.1063/1.4767517.
(156) Yang, W.; Ding, H.; Qi, G.; Li, C.; Xu, P.; Zheng, T.; Zhu, X.; Kenny, J. M.; Puglia, D.; Ma, P. Highly Transparent PVA/Nanolignin Composite Films with Excellent UV Shielding, Antibacterial and Antioxidant Performance. *React. Funct. Polym.* **2021**, *162* (March), 104873. https://doi.org/10.1016/j.reactfunctpolym.2021.104873.
(157) Li, X.; Hegyesi, N.; Zhang, Y.; Mao, Z.; Feng, X.; Wang, B.; Pukánszky, B.; Sui, X. Poly(Lactic Acid)/Lignin Blends Prepared with the Pickering Emulsion Template Method. *Eur. Polym. J.* **2019**, *110*, 378–384. https://doi.org/https://doi.org/10.1016/j.eurpolymj.2018.12.001.
(158) Benítez, A. J.; Torres-Rendon, J.; Poutanen, M.; Walther, A. Humidity and Multiscale Structure Govern Mechanical Properties and Deformation Modes in Films of Native Cellulose Nanofibrils. *Biomacromolecules* **2013**, *14* (12), 4497–4506. https://doi.org/10.1021/bm401451m.
(159) Fotie, G.; Limbo, S.; Piergiovanni, L. Manufacturing of Food Packaging Based on Nanocellulose: Current Advances and Challenges. *Nanomaterials* **2020**, *10* (9), 1–26. https://doi.org/10.3390/nano10091726.
(160) Wang, Y.; Wang, X.; Xie, Y.; Zhang, K. Functional Nanomaterials through Esterification of Cellulose: A Review of Chemistry and Application. *Cellulose* **2018**, *25* (7), 3703–3731. https://doi.org/10.1007/s10570-018-1830-3.
(161) Peng, S. X.; Chang, H.; Kumar, S.; Moon, R. J.; Youngblood, J. P. A Comparative Guide to Controlled Hydrophobization of Cellulose Nanocrystals via Surface Esterification. *Cellulose* **2016**, *23* (3), 1825–1846. https://doi.org/10.1007/s10570-016-0912-3.
(162) Missoum, K.; Belgacem, M. N.; Bras, J. Nanofibrillated Cellulose Surface Modification: A Review. *Materials (Basel).* **2013**, *6* (5), 1745–1766. https://doi.org/10.3390/ma6051745.
(163) Dufresne, A.; Belgacem, M. N. Cellulose-Reinforced Composites: From Micro- to Nanoscale. *Polimeros* **2013**, *23* (3), 277–286. https://doi.org/10.4322/polimeros.2010.01.001.
(164) Henriksson, M.; Berglund, L. A. Structure and Properties of Cellulose Nanocomposite Films Containing Melamine Formaldehyde. *J. Appl. Polym. Sci.* **2007**, *106* (4), 2817–2824. https://doi.org/https://doi.org/10.1002/app.26946.
(165) Lucenius, J.; Parikka, K.; Österberg, M. Nanocomposite Films Based on Cellulose Nanofibrils and Water-Soluble Polysaccharides. *React. Funct. Polym.* **2014**, *85*, 167–174. https://doi.org/https://doi.org/10.1016/j.reactfunctpolym.2014.08.001.
(166) Peresin, M. S.; Kammiovirta, K.; Heikkinen, H.; Johansson, L.-S.; Vartiainen, J.; Setälä, H.; Österberg, M.; Tammelin, T. Understanding the Mechanisms of Oxygen Diffusion through Surface Functionalized Nanocellulose Films. *Carbohydr. Polym.* **2017**, *174*, 309–317. https://doi.org/https://doi.org/10.1016/j.carbpol.2017.06.066.
(167) Aulin, C.; Gällstedt, M.; Lindström, T. Oxygen and Oil Barrier Properties of Microfibrillated Cellulose Films and Coatings. *Cellulose* **2010**, *17* (3), 559–574. https://doi.org/10.1007/s10570-009-9393-y.
(168) Martínez-Sanz, M.; Lopez-Rubio, A.; Lagaron, J. M. High-Barrier Coated Bacterial Cellulose Nanowhiskers Films with Reduced Moisture Sensitivity. *Carbohydr. Polym.* **2013**, *98* (1), 1072–1082. https://doi.org/https://doi.org/10.1016/j.carbpol.2013.07.020.
(169) Shimizu, M.; Saito, T.; Isogai, A. Water-Resistant and High Oxygen-Barrier Nanocellulose Films with Interfibrillar Cross-Linkages Formed through

Multivalent Metal Ions. *J. Memb. Sci.* **2016**, *500*, 1–7. https://doi.org/https://doi.org/10.1016/j.memsci.2015.11.002.
(170) Monot, F.; Borzeix, F.; Bardin, M.; Vandecasteele, J. Enzymatic Esterification in Organic Media: Role of Water and Organic Solvent in Kinetics and Yield of Butyl Butyrate Synthesis. *Appl. Microbiol. Biotechnol.* **1991**, *35*, 759–765.
(171) Ng, C. H.; Yang, K. L. Lipase in Biphasic Alginate Beads as a Biocatalyst for Esterification of Butyric Acid and Butanol in Aqueous Media. *Enzyme Microb. Technol.* **2016**, *82*, 173–179. https://doi.org/10.1016/j.enzmictec.2015.10.005.
(172) Perez, V. H.; da Silva, G. S.; Gomes, F. M.; de Castro, H. F. Influence of the Functional Activating Agent on the Biochemical and Kinetic Properties of Candida Rugosa Lipase Immobilized on Chemically Modified Cellulignin. *Biochem. Eng. J.* **2007**, *34* (1), 13–19. https://doi.org/10.1016/j.bej.2006.11.012.
(173) Gomes, F. M.; Pereira, E. B.; de Castro, H. F. Immobilization of Lipase on Chitin and Its Use in Nonconventional Biocatalysis. *Biomacromolecules* **2004**, *5* (1), 17–23. https://doi.org/10.1021/bm0342077.
(174) Al-Zuhair, S.; Jayaraman, K. V.; Krishnan, S.; Chan, W.-H. The Effect of Fatty Acid Concentration and Water Content on the Production of Biodiesel by Lipase. *Biochem. Eng. J.* **2006**, *30*, 212–217. https://doi.org/10.1016/j.bej.2006.04.007.
(175) Park, S.; Kim, S. H.; Kim, J. H.; Yu, H.; Kim, H. J.; Yang, Y. H.; Kim, H.; Kim, Y. H.; Ha, S. H.; Lee, S. H. Application of Cellulose/Lignin Hydrogel Beads as Novel Supports for Immobilizing Lipase. *J. Mol. Catal. B Enzym.* **2015**, *119*, 33–39. https://doi.org/10.1016/j.molcatb.2015.05.014.

Aalto-DD 69/2021

ISBN 978-952-64-0382-3 (printed)
ISBN 978-952-64-0383-0 (pdf)
ISSN 1799-4934 (printed)
ISSN 1799-4942 (pdf)

Aalto University
School of Chemical Engineering
Department of Bioproducts and Biosystems
www.aalto.fi

BUSINESS + ECONOMY

ART + DESIGN + ARCHITECTURE

SCIENCE + TECHNOLOGY

CROSSOVER

DOCTORAL DISSERTATIONS